Cobalamin riboswitches are broadly sensitive to corrinoid cofactors to enable an efficient gene regulatory strategy

Kristopher J. Kennedy[1], Florian J. Widner[1], Olga M. Sokolovskaya[1,2], Victoria L. Innocent[1], Rebecca R. Procknow[1], Kenny C. Mok[1], and Michiko E. Taga[1,*]

[1]Department of Plant and Microbial Biology, University of California, Berkeley, Berkeley, CA 94720, USA

[2]Present address: Department of Infectious Diseases, Genentech Inc., 1 DNA Way, South San Francisco, CA, 94080, USA

[*]Lead contact: taga@berkeley.edu

Summary

In bacteria, many essential metabolic processes are controlled by riboswitches, gene regulatory RNAs that directly bind and detect metabolites. Highly specific effector binding enables riboswitches to respond to a single biologically relevant metabolite. Cobalamin riboswitches are a potential exception because over a dozen chemically similar but functionally distinct cobalamin variants (corrinoid cofactors) exist in nature. Here, we measured cobalamin riboswitch activity *in vivo* using a *Bacillus subtilis* fluorescent reporter system and found that among 38 tested riboswitches, a subset responded to corrinoids promiscuously, while others were semi-selective. Analyses of chimeric riboswitches and structural models indicate that, unlike other riboswitch classes, cobalamin riboswitches indirectly differentiate among corrinoids by sensing differences in their structural conformation. This regulatory strategy aligns riboswitch-corrinoid specificity with cellular corrinoid requirements in a *B. subtilis* model. Thus, bacteria can employ broadly sensitive riboswitches to cope with the chemical diversity of essential metabolites.

Introduction

Controlling gene expression is an essential task that cells accomplish in a variety of ways. Non-coding RNAs are one such means of gene regulation, acting in parallel or in concert with historically better-studied protein-based mechanisms (Cech and Steitz, 2014). In bacteria and archaea, riboswitches are a widespread type of gene regulatory RNA with the distinct ability to sense particular intracellular metabolites by direct binding (Roth and Breaker, 2009). These RNAs are typically located in the 5'-untranslated region of mRNA transcripts and function as cis-regulators of downstream genes within their transcripts. A riboswitch is composed of an effector-binding aptamer domain and an expression platform. The aptamer domain adopts a three-dimensional structure that can bind its cognate effector molecule. The expression platform domain is a regulatory switch that interprets the effector-binding state of the upstream aptamer typically to promote or disrupt the transcription or translation of downstream genes (Winkler and Breaker, 2005). The diversity of riboswitch effectors and regulatory mechanisms has revealed fundamental insights into how bacteria sense and respond to dynamic environments and has also driven new approaches for precise control and manipulation of microbes for human purposes (Hallberg et al., 2017; Panchal and Brenk, 2021; Quereda and Cossart, 2017; Wrist et al., 2020).

Cobalamin (Cbl) riboswitches are among the most widespread and structurally diverse types of riboswitch in bacteria (McCown et al., 2017). They directly bind various forms of the enzyme cofactor Cbl as a cognate effector (Figure 1A, C) (Nahvi et al., 2002) to regulate genes involved in the biosynthesis, transport, and usage of Cbl. Cbl-dependent enzymes function in common metabolic pathways including methionine synthesis, deoxyribonucleotide synthesis, tRNA modification, and the degradation of certain amino acids, fatty acids, and biopolymers (Barker, 1985; Berg et al., 2007; Chang and Frey, 2000; Chen et al., 2001; Erb et al., 2008; Ferguson and Krzycki, 1997; Forage and Foster, 1982; Jeter, 1990; Korotkova et al., 2002; Krasotkina et al., 2001; Licht et al., 1996; Ljungdahl, 1986; Scarlett and Turner, 1976; Stupperich and Konle, 1993). Cbl is also required for rarer metabolic processes involved in antibiotic synthesis, mercury methylation, catabolism of steroids, and many others (Allen and Wang, 2014; Bridwell-Rabb et al., 2017; Choi and Bartha, 1993; Choi et al., 1994; Jost et al., 2015b; Kim et al., 2013; Knox et al., 2021; Marous et al., 2015; Parks et al., 2013; Pierre et al., 2012; Romine et al., 2017; Takano et al., 2011; Takano et al., 2015; Wang et al., 2020). Comparative genomic studies indicate that most bacteria perform Cbl-dependent metabolism and that Cbl-riboswitches often regulate these processes (McCown et al., 2017; Pavlova et al., 2019; Rodionov et al., 2003). However, an overlooked facet among most riboswitch studies is that Cbl is just one member of a class of enzyme cofactors known as corrinoids (Figure 1B) (Kennedy and Taga, 2020). In fact, Cbl-dependent enzymes in bacteria often function with corrinoids other than Cbl. Yet, it remains unclear whether the dozens of naturally occurring corrinoid cofactors are also Cbl-riboswitch effectors (Battersby, 2000; Chan and Escalante-Semerena, 2012; Hazra et al., 2015; Hoffmann et al., 2000; Moore et al., 2013; Newmister et al., 2012; Yan et al., 2018).

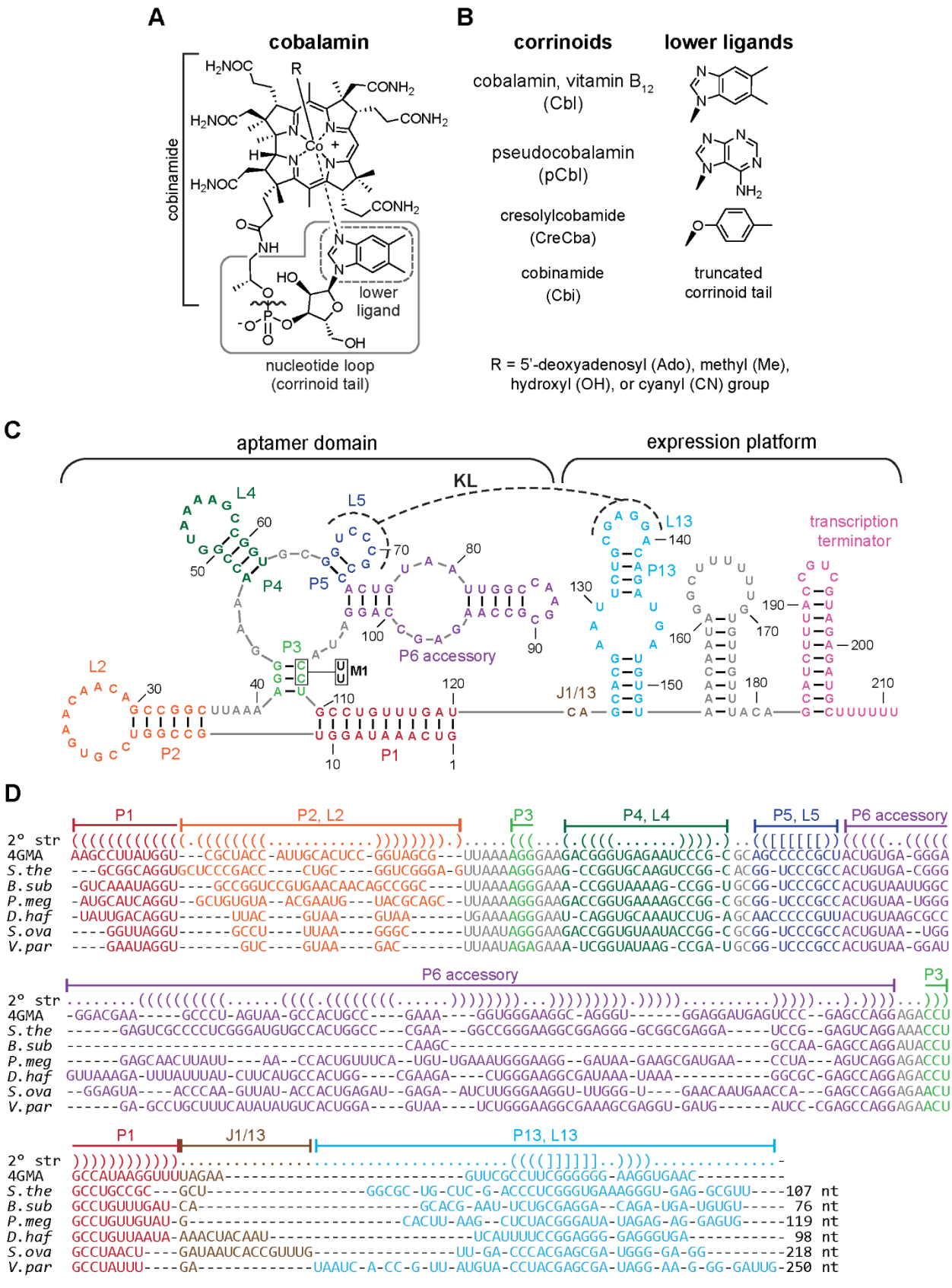
A
cobalamin
cobinamide
lower ligand
nucleotide loop (corrinoid tail)
B
corrinoids
lower ligands
cobalamin, vitamin B12 (Cbl)
pseudocobalamin (pCbl)
cresolylcobamide (CreCba)
cobinamide (Cbi)
truncated corrinoid tail
R = 5'-deoxyadenosyl (Ado), methyl (Me), hydroxyl (OH), or cyanyl (CN) group
C
aptamer domain
expression platform
KL
L4
L5
L13
P4
P5
P13
P3
P6 accessory
M1
L2
P2
P1
J1/13
transcription terminator
D
P1
P2, L2
P3
P4, L4
P5, L5
P6 accessory
2° str
4GMA
S.the
B.sub
P.meg
D.haf
S.ova
V.par
P6 accessory
P3
P1
J1/13
P13, L13
107 nt
76 nt
119 nt
98 nt
218 nt
250 nt

62

Figure 1 – Main corrinoids and riboswitches examined in this study. (A) Chemical structure of cobalamin, also called vitamin B_{12}. The gray solid line delineates the corrinoid tail region, which contains the variable lower ligand group in the gray dashed-line box. The R group is the upper ligand. (B) Names, lower ligand structures and abbreviations of the corrinoids used throughout this study. Cbl, pCbl and CreCba are 'complete corrinoids' (cobamides). Cbi is an 'incomplete corrinoid' that lacks the phosphoribosyl and lower ligand groups as indicated by the bracket and wavy line in the corrinoid tail in panel A. (C) Secondary structural model of the Cbl-riboswitch upstream of *B. subtilis btuF*. Base paired stems (P), loops (L), and junctions (J) are labeled. The P6 accessory region is highly variable in length and number of stems across Cbl-riboswitch sequences, often containing up to six paired regions. In this example, P6 accessory consists of only two paired regions. A kissing loop interaction (KL, dashed line) occurs between L5 of the aptamer and L13 of the expression platform. M1 indicates mutations C107U and C108U, which are examined in Figure 2F. (D) Secondary structural alignments of seven representative Cbl-riboswitches examined in this study. Row "2° str" indicates paired bases as parentheses, loops and junctions as periods, and kissing loop base pairs by brackets. PDB numbers or abbreviations are given for riboswitches from the following organisms and genes: 4GMA, *Thermanaerobacter tencongensis*; *S.the, Symbiobacterium thermophilum cblS*; *B.sub*, *B. subtilis btuF; P.meg*, *Priestia megaterium metE*; *D.haf*, *Desulfitobacterium hafniense* DSY0087; *S.ova*, *Sporomusa ovata btuB2*; *V.par*, *Veillonella parvula mutA*. Non-conserved sequences between P13 and the start codon are indicated by nucleotide sequence length (nt), but the actual sequences were omitted for clarity.

Corrinoid cofactors contain a highly substituted corrin ring with a central cobalt ion, a variable 'upper ligand' moiety coordinating the β axial face of the cobalt, and a tail structure extending from the corrin ring and terminating in a variable 'lower ligand' moiety that often coordinates the α axial face of the cobalt (Figure 1A, B). The molecular basis of selectivity of Cbl-riboswitches for upper ligand variants of Cbl has been relatively well studied, but selectivity for corrinoid tail variants remains mostly unexplored (Nahvi et al., 2002; Polaski et al., 2018; Polaski et al., 2017). To our knowledge, only one study has directly examined corrinoid tail specificity of a single Cbl-riboswitch. *In vitro* binding measurements showed that the aptamer of the *Escherichia coli btuB* Cbl-riboswitch binds the complete corrinoids Cbl and 2-methyladeninylcobamide ([2-MeAde]Cba) with a 3.2-fold difference in affinity (K_D = 89 and 290 nM, respectively). Furthermore, Cbi, an incomplete corrinoid with a truncated tail, binds the aptamer with roughly 8000-fold lower affinity than Cbl (K_D = 753 μM), suggesting that this aptamer binds corrinoids in a selective manner (Gallo et al., 2008). In light of these previous studies of corrinoid-specific metabolisms and Cbl-riboswitches, we hypothesize that Cbl-riboswitches harbor a range of distinct corrinoid tail-specific activities.

Here, we examined how a panel of 38 Cbl-riboswitches derived from 12 bacterial species responds to the distinct tail structures of four corrinoids: Cbl, pCbl, CreCba, and Cbi, representative of the benzimidazolyl, purinyl, phenolyl and incomplete corrinoids, respectively (Figure 1B). To compare activities among several dozen Cbl riboswitches, we devised a live cell fluorescence-based reporter system in *Bacillus subtilis*. In contrast to conventional *in vitro* biochemical approaches, this riboswitch reporter system captures the complete corrinoid-responsive gene regulatory process and provides rapid functional measurements with multiple effectors in parallel. Our results obtained from experiments in the reporter system in conjunction with comparative structural analyses of Cbl-riboswitches and corrinoid effectors allowed us to develop a mechanistic model for how corrinoid tail-specific gene regulation is achieved. Additionally, we examine a gene

regulatory strategy for the corrinoid specificity of a Cbl riboswitch and discuss the conceptual and practical implications of these findings.

Results

Experimental strategy – Development of an in vivo *reporter system*

In order to compare corrinoid selectivity among several Cbl-riboswitches and corrinoids, we constructed an *in vivo* GFP reporter system in *B. subtilis* that lacks other cellular factors that may interact with corrinoids. We engineered the strain to overexpress the Cbl uptake and adenosylation operon, *btuFCDR*, and deleted *queG*, which encodes the only Cbl-dependent enzyme in the genome. We found that *btuFCDR* overexpression increased uptake and adenosylation of not only Cbl, but also pCbl, CreCba and Cbi (Figure 2A-D). This strain is effective for measuring the response of the *B. subtilis btuF* Cbl-riboswitch to a broad range of concentrations of Cbl (Figure 2E-G). Notably, deletion of *btuR*, which encodes the adensosyltransferase that installs the Ado upper ligand group, rendered the *B. subtilis btuF* Cbl-riboswitch reporter insensitive to exogenously supplied CNCbl, MeCbl, and OHCbl, while retaining dose-dependent repression in response to AdoCbl (Figure S1). This strongly suggests that the *B. subtilis btuF* Cbl-riboswitch only responds to Cbl containing the 5'-deoxyadenosine upper ligand, in contrast with a report suggesting that this riboswitch aptamer can also bind MeCbl and OHCbl (Chan and Mondragón, 2020).

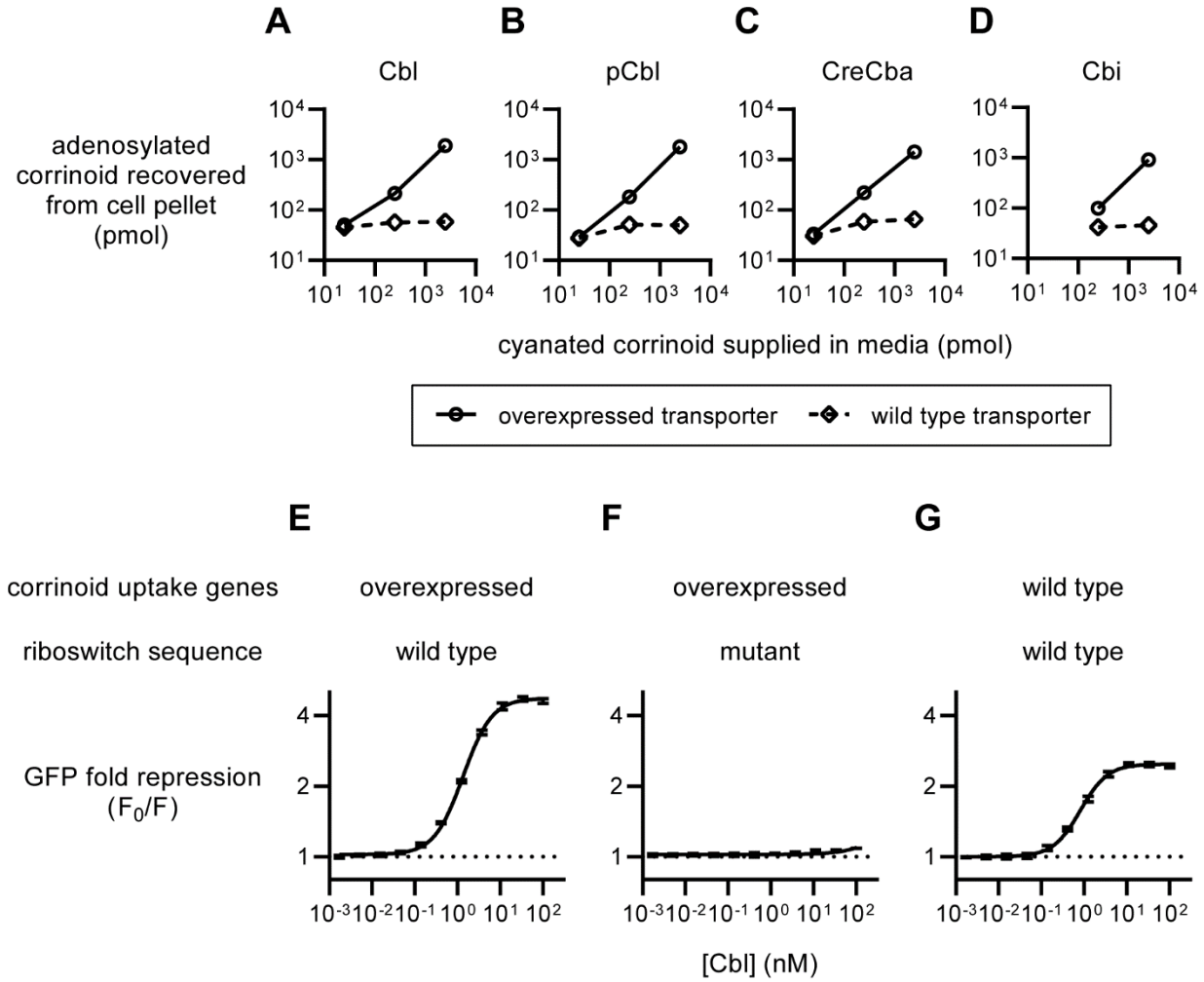

Figure 2 – Characterization of a live cell Cbl-riboswitch reporter system. (A-D) Intracellular accumulation of corrinoids in *Bacillus subtilis* strains containing the wild type (diamonds) or constitutively overexpressed (circles) corrinoid uptake genes *btuFCDR*. (E-G) Dose-responses of *B. subtilis btuF* GFP riboswitch reporters. 'Mutant' riboswitch refers to the M1 mutant version of the *B. subtilis btuF* riboswitch (Fig. 1C). Data points in panels A-D represent single measurements from one representative experiment. Data points and error bars in panels E-G represent mean and standard deviation of four independent replicates, and horizontal dotted lines demarcate no change in expression.

107

108 *Comparison of corrinoid specificity among Cbl-riboswitches*

109 In the strain background described above, we constructed 86 reporter strains to examine
110 riboswitches from 20 bacterial species including 10 species known to produce or require specific
111 corrinoids. Of the 86 reporters, 38 repressed GFP expression 0.5-fold or greater in response to one
112 or more corrinoids. 37 of these 38 functional riboswitch expression platforms contain a predicted
113 intrinsic transcriptional terminator suggesting that they are transcriptional riboswitches. We
114 observed extensive variation in sequence length and nucleotide composition throughout the
115 aptamers and expression platforms of the 38 riboswitches that were functional in *B. subtilis* (Figure
116 1D). Nine of the functional riboswitches are from *Priestia* (formerly *Bacillus*) *megaterium*, which

117 produces Cbl (Moore et al., 2013), and 12 are from *Sporomusa ovata* and *Veillonella parvula*
118 which both produce CreCba (Chan and Escalante-Semerena, 2012; Crofts et al., 2013; Newmister
119 et al., 2012; Stupperich et al., 1988). These results show that Cbl-riboswitches of diverse sequence
120 composition and origin can be examined with the *in vivo* reporter system. To address whether Cbl-
121 riboswitches are corrinoid selective, and how corrinoid selectivity varies among Cbl-riboswitches,
122 we measured the dose-responses of the 38 functional Cbl-riboswitches to four corrinoids, Cbl,
123 pCbl, CreCba and Cbi. Our results show that all of the riboswitches responded to more than one
124 corrinoid, and a subset responded to all four (Figure 3). Strikingly, all of the tested riboswitches
125 are either semi-selective (responding to more than one corrinoid) or promiscuous (responding to
126 all four corrinoids) (Figure 3A-B). We did not find any highly selective riboswitches that respond
127 to only one corrinoid. The semi-selective and promiscuous riboswitches all respond to Cbl and
128 pCbl (Figure 3C), and the promiscuous riboswitches additionally respond to Cbi and CreCba
129 (Figure 3D-E, points above the horizontal dashed line). Furthermore, the semi-selective
130 riboswitches are generally more sensitive to Cbl than to pCbl, while the promiscuous riboswitches
131 respond similarly to these two corrinoids. Almost all of the riboswitches respond weakly to CreCba
132 compared to the other three corrinoids (Figures S2-S4). In general, corrinoid selectivity appears to
133 be associated with taxonomic origin (Figure 3C-E). The riboswitches from the Bacilli class are
134 exclusively semi-selective (Figure S2), whereas those from Negativicutes are predominantly
135 promiscuous (Figure S3). The *S. ovata cobT* riboswitch is a notable exception that will be
136 discussed below. In contrast to taxonomy, corrinoid selectivity is not strongly associated with the
137 function of its regulatory target genes (Figure S5).

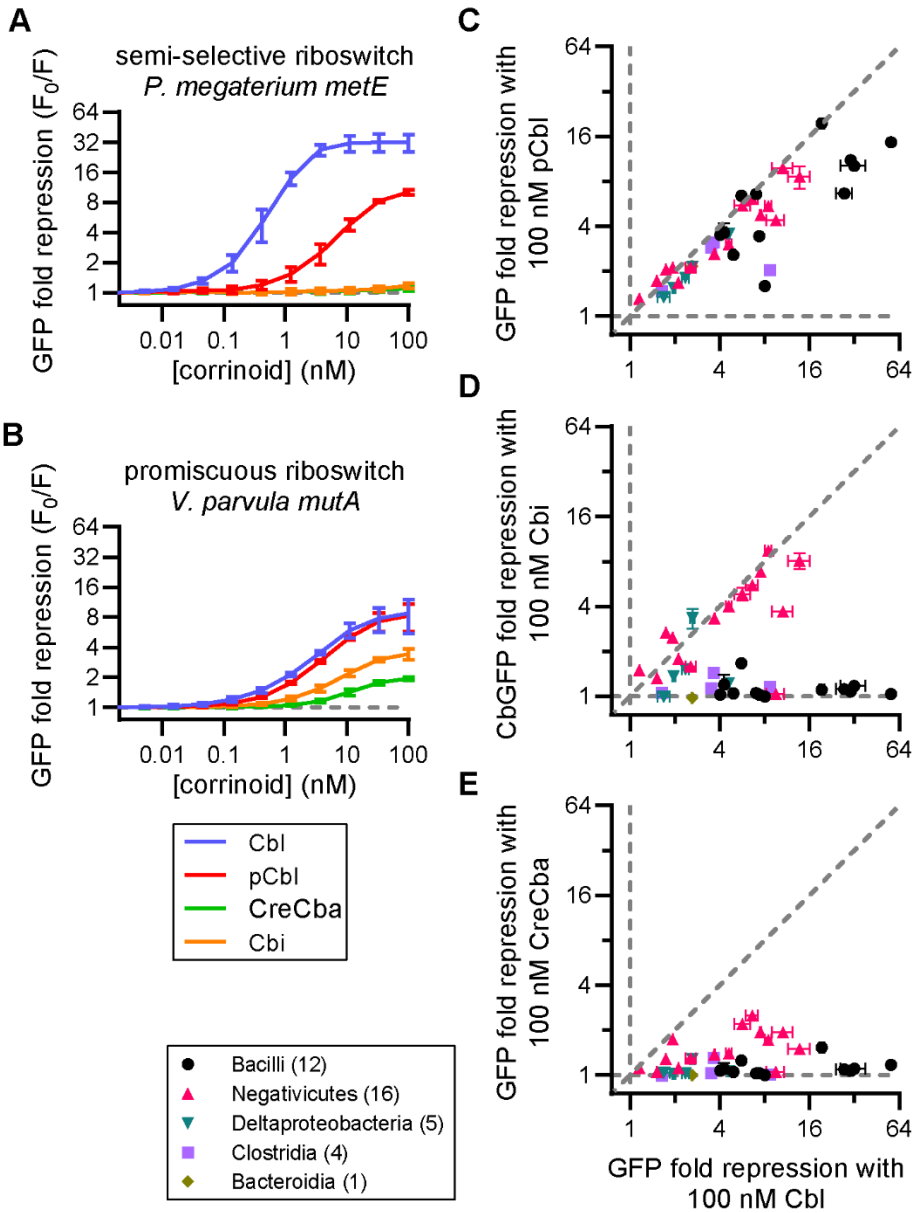

Figure 3 – Corrinoid specificity among 38 Cbl-riboswitches. (A,B) Corrinoid dose-responses of two riboswitch reporter strains with distinct corrinoid specificities, representing the semi-selective (A) and promiscuous (B) types. (C-E) Pairwise comparisons of GFP fold repression induced by 100 nM Cbl versus (C) pCbl, (D) Cbi, and (E) CreCba. Data points are colored by taxonomic class with the number of riboswitches analyzed from each class indicated in parentheses. Vertical and horizontal gray dashed lines demarcate a response to only one of the two corrinoids. Diagonal line demarcates equal response to two corrinoids. Data points and error bars in panels A and B represent mean and standard deviation of ten experiments for *P. megaterium metE* and six experiments for *V. parvula mutA*. Data points and error bars in panels C-E represent mean and range of at least two independent experiments for each riboswitch.

140 Next, we attempted to identify the RNA sequence features that underlie corrinoid selectivity.
141 Chimeric fusions of the semi-selective *P. megaterium metE* riboswitch and the promiscuous *V.*
142 *parvula mutA* riboswitch enabled us to examine the effects of specific domain and subdomain
143 sequences on corrinoid selectivity (Figure S6). Fusing the *P. megaterium metE* aptamer domain to
144 the expression platform of the *V. parvula mutA* riboswitch produced a semi-selective riboswitch
145 chimera, while the reciprocal chimera was promiscuous, suggesting that the aptamer domain is a
146 major determinant of corrinoid selectivity (Figure S6A). However, results from aptamer
147 subdomain swaps of stem P1, stem-loop P2-L2, stem-loop P4-L4, and P6 accessory region were
148 less conclusive. In the context of the *P. megaterium metE* riboswitch scaffold, swapping stem-loop
149 P2-L2 or the P6 accessory region with the corresponding structures of the *V. parvula mutA*
150 riboswitch produced chimeras that are less selective by gaining sensitivity to Cbi and CreCba
151 (Figure S6B). This suggests that these subdomains confer corrinoid promiscuity. Yet, within the
152 *V. parvula mutA* riboswitch scaffold, swapping stem P1 increased corrinoid selectivity by retaining
153 sensitivity to Cbl and pCbl, but losing sensitivity to CreCba and Cbi (Figure S6C). The remaining
154 chimeras partially or completely lost overall activity. These results demonstrate that subdomains
155 distributed throughout the aptamer domain may impact corrinoid selectivity; no single conserved
156 substructure completely controls corrinoid selectivity, nor did any single structure fully convert a
157 riboswitch's corrinoid selectivity. Thus, the source of the corrinoid selectivity phenotype appears
158 to be complex and requires inputs from multiple subdomains of the aptamer.

159 *Corrinoid tail structure impacts selectivity of Cbl-riboswitches*

160 We next sought to identify how structural differences in the corrinoid tail affect the response of
161 semi-selective Cbl-riboswitches to corrinoids. There are no predicted hydrogen bond interactions
162 between the lower ligand and the RNA in the X-ray crystal structures of Cbl-bound riboswitches,
163 making it difficult to surmise how a Cbl-riboswitch might distinguish between corrinoids (Chan
164 and Mondragón, 2020; Johnson et al., 2012; Peselis and Serganov, 2013). Could the overall
165 structural conformation of the corrinoid, rather than specific interactions between the RNA and
166 the corrinoid tail, influence Cbl-riboswitch activity? Most complete corrinoids exist in an
167 equilibrium between two distinct isomeric states known as 'base-on' and 'base-off' (Barker et al.,
168 1960; Ladd et al., 1961). In the base-on form, a nitrogen atom in the lower ligand base is
169 coordinated to the central cobalt atom of the corrin ring (as shown in Figure 1A). In the base-off
170 form, the cobalt ion is not coordinated by the nitrogen atom, allowing the tail to move more freely.
171 All six X-ray crystal structures of Cbl-riboswitches contain Cbl in the base-on form. The *E. coli*
172 *btuB* riboswitch aptamer was previously shown to bind Cbl with a higher affinity than the primarily
173 base-off corrinoids [2-MeAde]Cba and Cbi, yet [2-MeAde]Cba and Cbi were previously found to
174 remain primarily base-off while bound to the aptamer (Gallo et al., 2008). Interestingly, we noticed
175 that the semi-selective riboswitches respond strongly to Cbl and pCbl, which are capable of
176 switching between base-on and base-off forms, but respond weakly to Cbi or CreCba, which exist
177 exclusively in the base-off form. Additionally, we observe that semi-selective Cbl-riboswitches
178 are consistently more sensitive to Cbl, which has a greater base-on constitution than pCbl (Figures
179 3C, S2-S4). Based on these observations, we hypothesized that semi-selective riboswitches
180 specifically detect the base-on/off constitution of corrinoids. We therefore used a range of

181 corrinoids with diverse lower ligand structures to test whether the activity of Cbl-riboswitches
182 quantitatively correlates with the base-on/off constitution of the corrinoid.

183 We selected a panel of sixteen corrinoids for this analysis, including both natural and synthetic
184 benzimidazolyl, purinyl, and aza-benzimidazolyl corrinoids that span a range of base-on
185 tendencies between that of Cbl and pCbl (Figure S7). We observed a strong association between
186 base-on constitution – measured as the ratio of spectral absorbance at 525 and 458 nm in the
187 adenosylated form (Figure 4A) – and riboswitch response in semi-selective riboswitches (Figure
188 4B). Even among promiscuous Cbl-riboswitches, we observe measurable sensitivity to base-on
189 constitution, albeit to a much smaller degree (Figure 4C). These results support the hypothesis that
190 Cbl-riboswitches differentially regulate downstream gene expression by sensing corrinoid base-
191 on constitution.

192

193

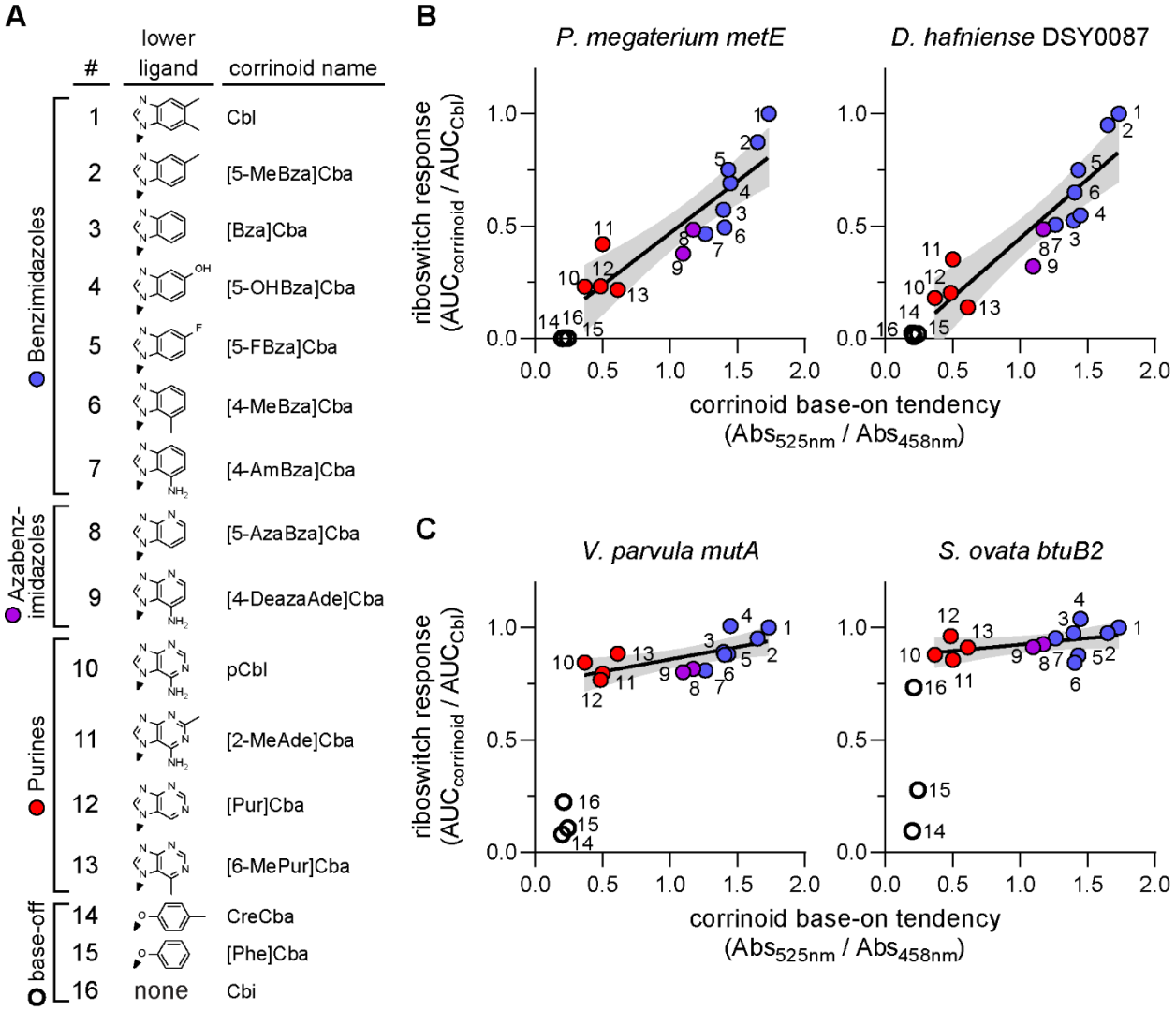

Figure 4 – Corrinoid base-on tendency correlates with corrinoid potency. (A) Sixteen adenosylated corrinoids used to test the relationship between corrinoid base-on tendency and corrinoid potency. (B) Semi-selective riboswitches *P. megaterium metE* and *D. hafniense* DSY0087 and (C) promiscuous riboswitches *V. parvula mutA* and *S. ovata btuB2* were used to measure the response to each corrinoid. Base-on tendency was measured as the ratio between spectral absorbance at 525 and 458 nm in a pH 7.3 solution. The cumulative corrinoid response was measured as the area under the dose-response curve of the riboswitch reporter strain for that corrinoid ($AUC_{corrinoid}$) relative to its dose-response to Cbl (AUC_{Cbl}). Corrinoids with benzimidazole (blue circles), azabenzimidazole (purple circles), and purine (red circles) lower ligands can adopt the base-on conformation. The corrinoids that are unable to adopt the base-on form (CreCba, [Phe]Cba and Cbi) are represented by empty circles. Trendlines in B and C were fit to data points of corrinoids with benzimidazole, azabenzimidazole and purine lower ligands, with strictly base-off corrinoids excluded. Each data point represents a single measurement of riboswitch dose-response and corrinoid base-on tendency.

194

Structural comparisons between base-on and base-off tail orientations

The results presented above led us to speculate about how a Cbl-riboswitch could detect the base-on constitution of a corrinoid. In all published X-ray crystal structures of Cbl-riboswitches, aptamer-effector binding is achieved mainly through van der Waals forces and shape complementarity between the binding site and base-on Cbl. Only a few hydrogen bonds between the RNA and corrinoid are observed, none of which occur with the lower ligand group of Cbl (Chan and Mondragón, 2020; Johnson et al., 2012; Peselis and Serganov, 2013). Thus, it appears unlikely that the riboswitch is directly detecting the specific chemical differences among corrinoid lower ligands. Instead, we considered whether the riboswitch discriminates base-on and base-off forms of a corrinoid by sensing corrinoid conformation. In the base-on form, the tail is spatially constrained due to the Co-N coordinate bond, whereas in the base-off form it is able to sample a wider range of spatial positions (Marques et al., 2000). To develop mechanistic insight into how the base-on/off constitution of a corrinoid could impact Cbl-riboswitch activity, we leveraged the plethora of publicly accessible X-ray crystal structures of macromolecule-bound Cbl (Berkovitch et al., 2004; Chan and Mondragón, 2020; Dowling et al., 2016; Drennan et al., 1994; Froese et al., 2010; Gruber et al., 2001; Johnson et al., 2012; Jost et al., 2015a; Jost et al., 2015b; Mancia et al., 1996; Payne et al., 2015a; Payne et al., 2015b; Peselis and Serganov, 2013; Sussman and Wilson, 2000). We first assessed the range of structural conformations that are potentially sampled by corrinoids as they dynamically switch between base-on and base-off states by aligning and visually comparing various structural models of Cbl. Six base-on Cbl models were obtained from structural studies of Cbl-riboswitches and synthetic Cbl RNA aptamers, whereas base-off/His-on Cbl models were obtained from X-ray crystal structures of ten Cbl-dependent enzymes (Supplemental Table 1). After aligning and superimposing these molecular models by their central cobalt and coordinating nitrogen atoms, we observed that the corrin rings and their amide and methyl substituents occupy similar spatial positions, but the tails of base-on and base-off Cbl structures occupy distinct positions (Figure 5A-B). Moreover, the base-on Cbl tails appear in very similar positions with lower ligands in close proximity to the central cobalt ion, whereas the base-off Cbl tails appear more scattered with lower ligands more distal to the cobalt ion. These structural alignments visually convey the degree to which the conformations of base-on and base-off corrinoids can vary among biomolecular complexes.

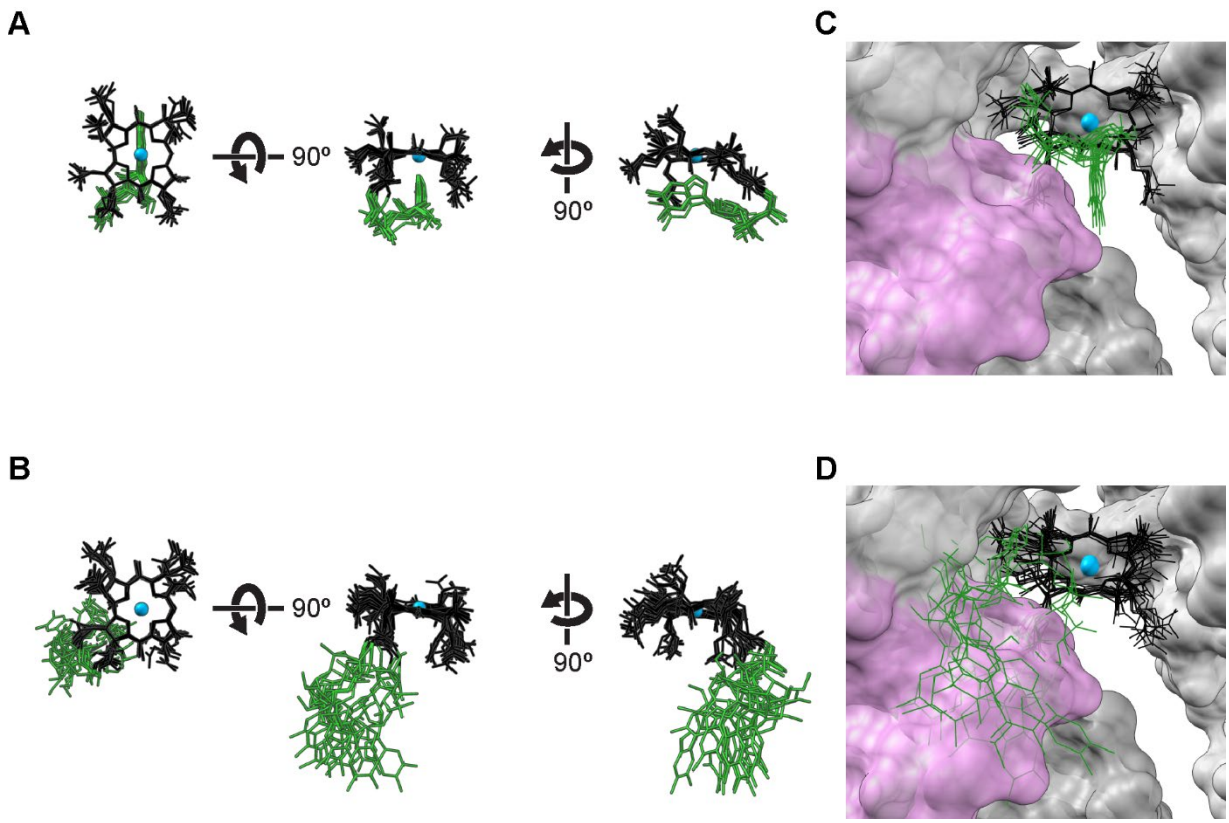

Figure 5 – Distinct tail positions among base-on and base-off corrinoids may impact binding of corrinoids to riboswitches. 3D alignments of Cbl structural models derived from published X-ray crystal structures of (A) base-on Cbl in complex with RNAs and (B) base-off Cbl in complex with proteins. The Cbl-binding site in the X-ray crystal structure of the *Thermoanaerobacter tengcongensis* Cbl-riboswitch (PDB ID 4GMA) is depicted with (C) base-on and (D) base-off Cbl alignments. Cbl models were aligned by the cobalt and coordinating nitrogen atoms in the corrin ring. Structures of the corrin ring, cobalt, and tail of Cbl are colored in black, blue, and green, respectively. Upper ligand structures of Cbl were omitted for clarity. Riboswitch RNA structures are depicted as space-filled models with the L5-L13 kissing loop in pink and the rest of the RNA in gray.

Next, we compared the positions of the aligned base-on and base-off Cbl models in the context of 3D Cbl-riboswitch models. We analyzed X-ray crystal structures of the two Cbl-riboswitches that contain resolved kissing loop structures: one from *Thermoanaerobacter tengcongensis* (Figure 5C-D) and one identified from a marine metagenome sequence (Figure S8A-B) (Johnson et al., 2012). These structural models show that the base-on tails are contained within the binding site, whereas the tails of the base-off Cbl structures protrude away from the binding site and clash with the L5-L13 kissing loop. Although the *B. subtilis btuF* (Figure S8C-D) and *Symbiobacterium thermophilum cblT* (Figure S8E-F) riboswitch models do not contain the L13 structure of the kissing loop, some of the modeled base-off tails clash with L5 of the aptamer in these structures (Chan and Mondragón, 2020; Peselis and Serganov, 2013). The kissing loop has been shown to play a key mechanistic role of sensing the corrinoid-binding state of the aptamer domain to

238 influence downstream regulatory structures in the expression platform (Lussier et al., 2015;
239 Polaski et al., 2016). If kissing loop formation in semi-selective Cbl-riboswitches is sensitive to
240 the base-on/off constitution of the corrinoid, then corrinoid selectivity may be mediated by either
241 selective binding by the aptamer or selective formation of downstream regulatory structures.

242 To determine whether the expression platform structures can impact corrinoid selectivity, we
243 examined corrinoid-selective binding separately from subsequent corrinoid-selective regulation.
244 We tested for promiscuous binding by comparing the Cbl dose-response of the *P. megaterium*
245 *metE* Cbl-riboswitch in the presence and absence of competing 100 nM Cbi and found that the
246 response to Cbl is unaffected by Cbi (Figure S9A-B). This indicates that Cbi does not compete
247 with Cbl for riboswitch binding, supporting corrinoid-selective binding as the mechanism of semi-
248 selectivity. However, when the aptamer of this semi-selective riboswitch is replaced with the
249 aptamer of the promiscuous *S. ovata nikA* riboswitch, it retains semi-selectivity, which suggests
250 that the *P. megaterium* expression platform also plays a role in corrinoid selectivity (Figure S9A).
251 Interestingly, the Cbl dose-response of the *S. ovata nikA* / *P. megaterium metE* chimeric riboswitch
252 does become sensitized to competing Cbi addition, confirming that the *S. ovata nikA* aptamer
253 retains sensitivity to base-off corrinoid in the context of this chimera (Figure S9C). Taken together,
254 these results show that base-off corrinoids may impede both Cbl-riboswitch binding and formation
255 of regulatory structures, explaining the link between base-on/off constitution and riboswitch
256 activity observed in Figure 4.

257 *Gene regulatory strategy of corrinoid selectivity*

258 While the prior experiments clearly demonstrate that Cbl-riboswitches are capable of
259 distinguishing between corrinoids, we wondered what purpose Cbl-riboswitch corrinoid selectivity
260 might serve in the organisms containing these regulatory systems. We posit that Cbl-riboswitch
261 selectivity reflects a regulatory strategy that complements the corrinoid-specific requirements of
262 the cell and avoids gene mis-regulation. As a specific example, we hypothesize that only corrinoids
263 that are functionally compatible with a Cbl-dependent enzyme should cause riboswitch-mediated
264 repression of the expression of its Cbl-independent counterpart (Figure 6A, B). We tested this
265 hypothesis directly in *B. subtilis* by examining the function and regulation of methionine synthase
266 isozymes MetE (Cbl-independent) and MetH (Cbl-dependent), which are commonly found in
267 bacterial genomes with a Cbl-riboswitch upstream of the *metE* gene (Mukherjee et al., 2019;
268 Sudarsan et al., 2006). The *B. subtilis* genome contains *metE* but lacks *metH*, and no Cbl-
269 riboswitch is located upstream of *metE*. We therefore constructed strains of *B. subtilis* that
270 heterologously express the *metE* or *metH* locus from the related species *P. megaterium*, in a Δ*metE*
271 background with overexpressed corrinoid uptake genes (Figure 6C). In each strain, the *P.*
272 *megaterium* genes are constitutively transcribed from the promoter P_{Veg} and also contain a
273 transcriptionally fused *gfp* to measure expression levels. Growth of the *B. subtilis* strain expressing
274 *P. megaterium metH* in a medium lacking methionine was supported to varying extents by most
275 benzimidazolyl and both phenolyl cobamides, but not by [5-OHBza]Cba, the purinyl cobamides,
276 or Cbi (Figure 6C, red squares). This result indicates that MetH-dependent growth is influenced
277 by the corrinoid tail structure, as observed previously in other bacteria (Degnan et al., 2014;
278 Helliwell et al., 2016; Ma et al., 2020; Sokolovskaya et al., 2019; Tanioka et al., 2010). In the *B.*

279 *subtilis* strain containing the *P. megaterium metE* gene and repressing Cbl-riboswitch, growth was
280 suppressed by benzimidazolyl cobamides to different extents (Figure 6C, blue circles). This
281 growth pattern coincides with the GFP repression measured for the *metE* riboswitch (Figure S10),
282 except that the repression of *metE* by purinyl cobamides is apparently insufficient to suppress
283 growth in this context. Comparison of the two strains in response to a suite of corrinoids reveals a
284 striking correspondence between riboswitch-mediated suppression of growth in the *metE*-
285 containing strain and growth promotion by corrinoids in the *metH*-containing strain (Figure 6C).
286 [5-OHBza]Cba and the phenolyl cobamides are exceptions to the trend, though in neither case is
287 MetE-dependent growth completely suppressed by a corrinoid incompatible with MetH. This
288 result demonstrates that riboswitch-based repression and cobalamin-dependent isozyme function
289 are largely aligned for the *P. megaterium metE*-*metH* pair and suggests that Cbl-riboswitch
290 specificity may generally adhere to a regulatory strategy reflecting the cell's corrinoid preference.

291

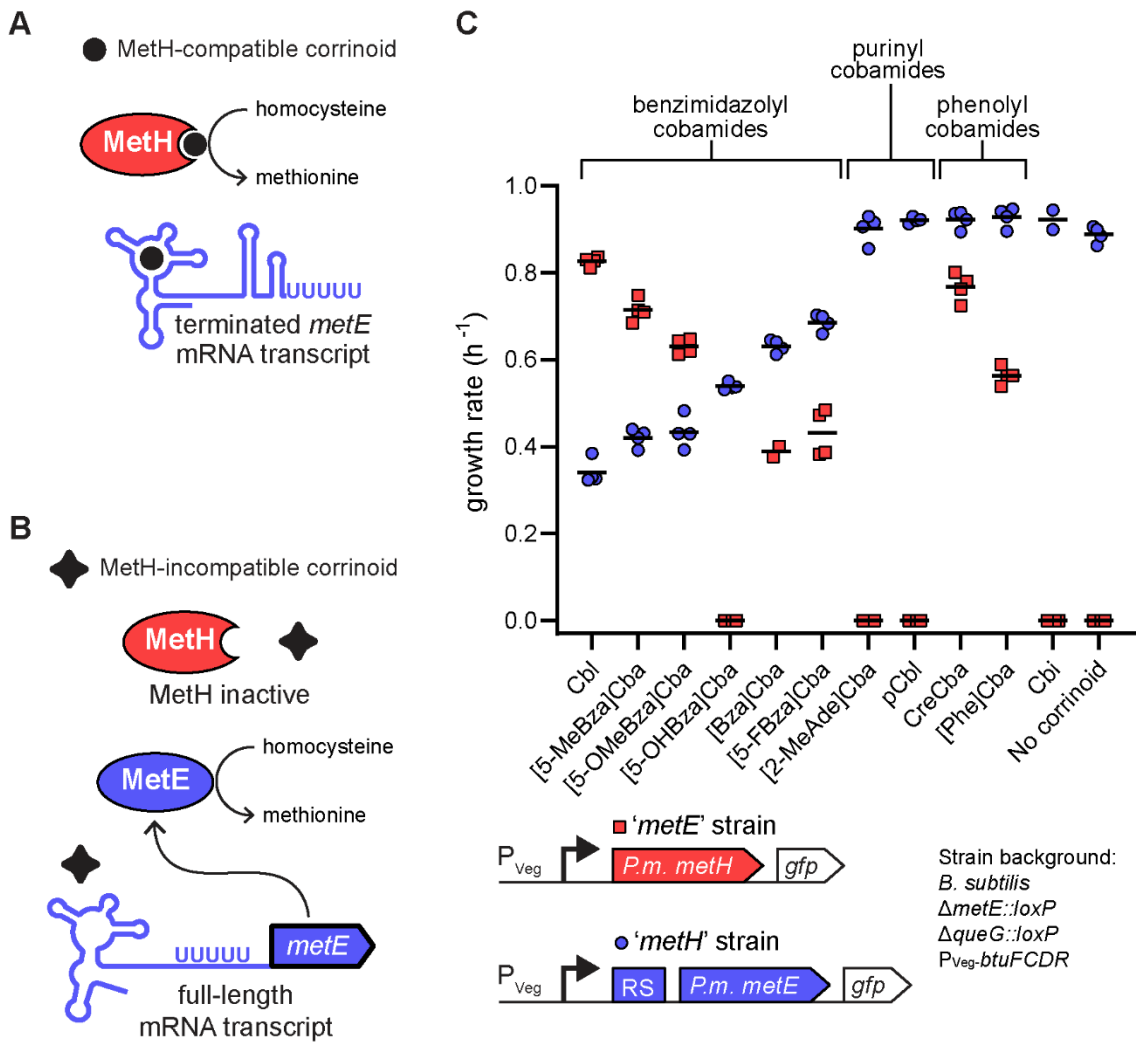

292

Figure 6 – Corrinoid specificities of the *P. megaterium metE* riboswitch and *P. megaterium* MetH enzyme are aligned. Expression of the Cbl-independent methionine synthase MetE and enzymatic activity of the Cbl-dependent methionine synthase MetH are potentially impacted by the presence of (A) MetH-compatible corrinoids and (B) MetH-incompatible corrinoids. (C) The '*metH*' strain (red) is a *B. subtilis* Δ*metE::loxP* Δ*queG::loxP* P_{Veg}-*btuFCDR* strain heterologously expressing *P. megaterium metH*. The '*metE*' strain (blue) is a *B. subtilis* Δ*metE::loxP* Δ*queG::loxP* P_{Veg}-*btuFCDR* strain heterologously expressing *P. megaterium metE* downstream from a SAM-Cbl tandem riboswitch (RS). Each methionine synthase gene is constitutively expressed from the P_{Veg} promoter and is transcriptionally fused to *gfp*. Growth rates of the '*metE*' (blue circles) and '*metH*' (red squares) strains were measured in methionine-dependent culture conditions containing 20 nM corrinoid. Data points are individual growth rate measurements and black horizontal lines represent the mean of the four replicate measurements.

293

Discussion

Riboswitches are key regulators of microbial gene expression. The Cbl-riboswitch was the first type discovered and is among the most widely distributed riboswitch classes in bacteria and archaea (Nahvi et al., 2004; Nahvi et al., 2002). Previous biochemical and structural studies have uncovered the major molecular features of the Cbl-riboswitch response to Cbl (Chan and Mondragón, 2020; Gallo et al., 2011; Johnson et al., 2012; Lussier et al., 2015; Peselis and Serganov, 2013; Polaski et al., 2016; Polaski et al., 2018; Polaski et al., 2017; Sudarsan et al., 2006). Yet few studies have examined how other naturally occurring corrinoids impact gene regulation by Cbl-riboswitches (Gallo et al., 2008). Here, we found that Cbl-riboswitches vary in their ability to discriminate between corrinoids, with some being semi-selective on the basis of corrinoid base-on/off state, and others being promiscuous. These results were enabled by a carefully designed fluorescent reporter system capable of measuring the responses of dozens of Cbl-riboswitches to multiple corrinoids *in vivo* (Figures 2, S1).

We observed that Cbl-riboswitches display different degrees of corrinoid selectivity, with some that respond to a subset of corrinoids (semi-selective) and others that respond to all tested corrinoids (promiscuous) (Figures 3, S2-S4). Our chimeric riboswitch results suggest that sequence and structural determinants of corrinoid selectivity are dispersed throughout the Cbl-riboswitch aptamer scaffold rather than being confined to a single conserved region (Figure S6). This finding contrasts with other studies of riboswitch specificity. For example, in a study of Cbl upper ligand specificity, a few key residues in the Cbl binding site were sufficient to fully convert a Cbl-riboswitch from MeCbl-specific to AdoCbl-specific (Polaski et al., 2017). In purine riboswitches, effector specificity is achieved by positioning of a critical conserved uracil or cytosine residue in the binding site of the aptamer, which forms a base-pair with the adenine or guanine effector, respectively. Among the various families of SAM riboswitches, highly specific binding of SAM and exclusion of SAH is achieved by RNA structures that discriminate the charged sulfonium ion of SAM from the uncharged sulfoether of SAH (Price et al., 2014). In contrast, the SAM/SAH riboswitch class attains effector promiscuity for SAM and SAH by a general lack of interaction between the RNA and the aminocarboxypropyl side chains of these effectors (Huang et al., 2020; Weickhmann et al., 2019). This is reminiscent of Cbl-riboswitches which similarly have few molecular contacts between the RNA and corrinoid tail (Gallo et al., 2011; Gallo et al., 2008; Johnson et al., 2012; Peselis and Serganov, 2013).

Overall, our structural model analyses support a mechanism in which semi-selective Cbl-riboswitches primarily sense the distinct corrinoid tail orientations of the base-on and base-off forms. In this case, Cbl-riboswitches only indirectly sense the chemical composition of the variable lower ligand group, with differential binding largely determined by steric effects and shape complementarity (Figures 4-5). Recent molecular dynamics simulations of the *T. tengcongensis* Cbl-riboswitch suggest that the kissing loop structure may form prior to effector binding, which would place even greater constraints on the corrinoid tail orientation to achieve shape complementarity with its binding site (Ma et al., 2021). Additionally, some Cbl-riboswitches may in fact bind base-off corrinoids but disrupt subsequent formation of downstream regulatory structures of the expression platform, perhaps by interfering with the kissing loop (Figure S9). A

335 similar feature has been observed in tetrahydrofolate (THF) riboswitches where chemical
336 variations in the para-aminobenzoic acid moiety of THF analogs differentially perturb expression
337 platform structures without affecting aptamer binding (Trausch and Batey, 2014). The mechanisms
338 of corrinoid selectivity of Cbl-riboswitches could be directly tested in future structural or
339 biochemical studies of promiscuous Cbl-riboswitches with base-on and base-off corrinoids.

340 In regard to gene regulatory strategies, it seems sensible that Cbl-riboswitches are not highly
341 effector-specific because bacteria are often flexible in their corrinoid usage. A variety of corrinoids
342 have been shown to support growth of *C. difficile*, *S. ovata, and Ensifer meliloti* despite each of
343 these organisms displaying highly specific corrinoid production (Mok and Taga, 2013; Shelton et
344 al., 2020; Sokolovskaya et al., 2019). Furthermore, since corrinoid auxotrophy is prevalent among
345 corrinoid-dependent bacteria, many organisms may need to take advantage of the wide range of
346 corrinoids that may be available in their environment (Shelton et al., 2019). Thus, the range of
347 effector selectivity that we observe among Cbl-riboswitches may reflect a coevolution between
348 corrinoid-responsive gene regulation and corrinoid-dependent physiology. Our result
349 demonstrating complementary corrinoid selectivity between *P. megaterium* MetH-dependent
350 growth and Cbl-riboswitch-dependent expression of MetE is consistent with this notion (Figure
351 6).

352 Alternatively, the preference for corrinoid base-on constitution among Cbl-riboswitches may
353 function as a proxy to discriminate complete corrinoid coenzymes from incomplete corrinoids such
354 as Cbi, which often function poorly as coenzymes. This idea has been proposed as an explanation
355 for the remarkably high selectivity of the corrinoid uptake system in mammals (Fedosov et al.,
356 2007). Interestingly, we found that all but one of the *S. ovata* riboswitches tested are promiscuous
357 types that can respond to its natively produced CreCba. The notable exception is a semi-selective
358 riboswitch upstream of the gene *cobT* (Figure S3), which functions in a late step of corrinoid
359 biosynthesis that occurs after synthesis of Cbi (Chan et al., 2014; Cheong et al., 1999, 2001; Crofts
360 et al., 2013; Hazra et al., 2013; Trzebiatowski and Escalante-Semerena, 1997; Trzebiatowski et
361 al., 1994). Thus, this Cbl-riboswitch that discriminates against Cbi may allow homeostatic
362 regulation of *cobT* in response to complete corrinoids like Cbl, while preventing unproductive
363 repression of *cobT* in the presence of incomplete corrinoids like Cbi. Future studies examining
364 corrinoid-specific gene regulation of riboswitches in the context of their native organisms may
365 help clarify which regulatory strategies are generally at play in corrinoid-related bacterial
366 physiology.

367 There is significant interest in the fields of bioengineering and synthetic biology to use
368 riboswitches as gene regulatory devices because they act more rapidly and efficiently than protein-
369 based regulatory systems (Galizi and Jaramillo, 2019; Hallberg et al., 2017; Villa et al., 2018;
370 Wrist et al., 2020). Riboswitches have also become desirable therapeutic drug targets because they
371 often control essential metabolic pathways in pathogenic microbes (Mansjö and Johansson, 2011;
372 Panchal and Brenk, 2021; Quereda and Cossart, 2017). Broader consideration of the
373 conformational dynamics of larger types of effector molecules including organic cofactors,
374 antibiotics, and their analogs could aid efforts to engineer synthetic RNA-based regulatory
375 platforms that function robustly *in vivo*. This could also inform future efforts to develop synthetic

376 antimetabolites that, for example, elicit gene mis-regulation, instead of a more common strategy
377 of creating inhibitors for enzymes (Kräutler, 2020; Zelder et al., 2015).

378 The chemical diversity of corrinoids is intrinsically linked to a vast array of metabolic processes
379 and microbial interactions. Yet it remains unclear how microbes have evolved to cope with and
380 thrive on the assortment of natural corrinoid analogs, especially when compared to other primary
381 metabolites including organic cofactors, nucleotides and amino acids which typically require one
382 specific structural form for precise biological functions. We have gained new appreciation for the
383 impacts of chemical diversity on biological function by focusing on the Cbl-riboswitch with its
384 distinctively complex structure and regulatory mechanism, and by accounting for the often
385 overlooked biological and ecological roles of corrinoid analogs. Future studies into the evolution
386 of microbial molecular specificity for corrinoids may yield further insight into the nature of these
387 exceptionally versatile coenzymes.

388

389 **Materials and methods**

390 *Cbl-riboswitch sequence analysis*

391 Cbl-riboswitch sequences, chromosomal coordinates and regulon information were downloaded
392 from the RiboD online database (Mukherjee et al., 2019) (Supplemental File 1). The genome of
393 *Sporomusa ovata* was not included in the RiboD database, so we used the RiboswitchScanner
394 webserver to search for Cbl-riboswitches in this organism (Mukherjee and Sengupta, 2016; Singh
395 et al., 2009). Cbl-riboswitch aptamer sequences were manually aligned by conserved secondary
396 structures bounded by the 5' and 3' ends of the P1 stem (Choudhary et al., 2013; McCown et al.,
397 2017) (Supplemental File 2). The P13-L13 stem loop and potential intrinsic transcriptional
398 termination hairpin structures of the expression platform were identified using secondary structure
399 prediction tools in RNAstructure 6.2 (Mathews et al., 2004; Reuter and Mathews, 2010). Intrinsic
400 terminators were identified as stem loops directly preceding a sequence of five or more consecutive
401 uracil residues (Gusarov and Nudler, 1999; Wilson and von Hippel, 1995). Sequence alignment
402 and annotation was carried out in JalView 2.11.1.4 (Waterhouse et al., 2009). Cartoons of
403 riboswitch secondary structures were constructed using the StructureEditor program of
404 RNAstructure 6.2 (Reuter and Mathews, 2010).

405 *Corrinoid production, extraction, purification, and analysis*

406 Cyanocobalamin, adenosylcobalamin, methylcobalamin, hydroxocobalamin, and
407 dicyanocobinamide were purchased from MilliporeSigma. All other corrinoids used in this study
408 were produced in bacterial cultures and purified in cyanated form as previously described (Mok
409 and Taga, 2013; Sokolovskaya et al., 2019; Sokolovskaya et al., 2020; Yi et al., 2012). For the
410 experiments in Figures 4 and S7, corrinoids other than cobalamin were chemically adenosylated
411 to obtain the coenzyme (5'-deoxyadenosylated) form as previously described (Sokolovskaya et al.,
412 2019; Sokolovskaya et al., 2020).

413 UV/Vis spectra were collected from corrinoid samples in UV/Vis-transparent 96-well microtiter
414 plates (greiner bio-one UV-STAR® 675801) using a BioTek Synergy 2 or Tecan Infinite M1000

415 Pro plate reader. To measure concentrations of corrinoid stock solutions, corrinoid samples were
416 diluted 10-fold in 10 mM sodium cyanide to obtain the dicyanated base-off form of the corrinoid.
417 The concentration of the dicyanated corrinoid was calculated using the extinction coefficient ε580
418 = 10.1 mM^{-1} cm^{-1} (Mok et al., 2020; Stupperich et al., 1988). For adenosylated corrinoids used in
419 Figures 4 and S7, base-on/off constitution at neutral pH was measured as the ratio of spectral
420 absorbance at 525 nm and 458 nm in phosphate buffered saline solution pH 7.3 at 37°C (Fieber et
421 al., 2002; Hoffmann et al., 2000).

422 *Plasmid and strain construction*

423 Plasmids generated in this study were constructed with one-step isothermal assembly (Gibson et
424 al., 2009) and introduced into *E. coli* strain XL1-Blue by heat shock transformation. Riboswitch
425 reporter plasmids were constructed in the shuttle vector pSG13 (Guiziou et al., 2016). Riboswitch
426 DNA sequences were inserted between the transcriptional start site of the constitutive P_{Veg}
427 promoter and the *gfp* translational start site of pSG13. For riboswitch sequences that resulted in no
428 detectable GFP signal under any conditions, a synthetic ribosome binding site (RBS) sequence R0
429 (5'-GATTAACTAATAAGGAGGACAAAC-3') from pSG13 was placed between the riboswitch
430 sequence and *gfp* translational start site (Supplemental File 1).

431 Strains used in this study are listed in Supplemental File 3. All *B. subtilis* riboswitch fluorescent
432 reporter strains and *B. subtilis* strains expressing *P. megaterium metE* and *metH* used in this study
433 are derived from the high-efficiency transformation strain SCK6, which has a xylose-inducible
434 competence gene cassette (Zhang and Zhang, 2011). Preparation of competent cells and
435 transformations of all SCK6-derived strains were performed as previously described (Zhang and
436 Zhang, 2011). The strain KK642, which overexpresses the corrinoid uptake genes, was constructed
437 by deletion of gene *queG* and replacement of the promoter and 5' untranslated region of the
438 *btuFCDR* operon with the P_{Veg} promoter and R0 RBS (Guiziou et al., 2016). *B. subtilis* genes
439 *queG*, *btuR*, and *metE* were targeted for deletion by recombination with kanamycin resistance
440 cassettes containing flanking sequence homology to each respective locus. Kanamycin resistance
441 cassettes were PCR-amplified from genomic DNA of *B. subtilis* strains BKK08910
442 (Δ*queG*::kan^R), BKK33150 (Δ*btuR*::kan^R), and BKK13180 (Δ*metE*::kan^R) (Koo et al., 2017).
443 Kanamycin resistance cassettes were removed by Cre-Lox recombination using plasmid pDR244
444 as previously described (Koo et al., 2017).

445 *B. subtilis* strains heterologously expressing *metE* and *metH* from *P. megaterium* were constructed
446 as follows. The *metE* and *metH* genes were PCR-amplified from genomic DNA of *P. megaterium*
447 DSM319 and cloned between the transcriptional start site and the *gfp* translational start site of
448 pSG13. The *P. megaterium metE* amplified fragment starts at the SAM-Cbl tandem riboswitch in
449 the 5' UTR and ends at the *metE* stop codon, whereas the *P. megaterium metH* fragment starts at
450 the *metH* RBS, which is composed of 20 nucleotides preceding the *metH* translational start site
451 and ends at the *metH* stop codon.

452 Riboswitch reporter plasmids and plasmids containing *P. megaterium metE* and *metH* were
453 linearized by restriction enzyme digest with ScaI-HF (New England Biolabs) and selected for
454 integration at the *amyE* locus of *B. subtilis* by plating on lysogeny broth (LB) agar with 100 µg/mL

455 spectinomycin. Colonies were screened for integration at *amyE* by colony PCR. All stocks of
456 bacterial strains were stored in 15% glycerol at -80 ºC.

457 *Intracellular corrinoid accumulation experiments*

458 *B. subtilis* strains were inoculated from single colonies into 50 mL LB and grown with aeration at
459 37 ºC in a shaking incubator (Gyromax 737R, Amerex Instruments, Inc.) for 5-6 hours until
460 reaching an optical density at 600 nm (OD_{600}) of 1.0 to 1.5. Each culture was diluted 10-fold in
461 LB and split into 13 25 mL cultures containing 0, 25, 250, or 2500 picomoles of a cyanated
462 corrinoid (Cbl, pCbl, CreCba and Cbi). These cultures were incubated at 37 ºC with aeration for
463 3-4 hours to a final OD_{600} of 1.5 to 2.0. The cells were pelleted by centrifugation at 4,000 g for 10
464 min. Cell pellets were rinsed three times by resuspension in 10 mL phosphate buffered saline
465 solution pH 7.3 followed by centrifugation. After the final centrifugation, tubes were wrapped in
466 aluminum foil to protect adenosylated corrinoids from exposure to light.

467 To extract intracellular corrinoids, cell pellets were resuspended in 5 mL of 100% methanol by
468 vigorous vortexing for 30 secs. Samples were stored at -80 ºC until the next day. Frozen lysates
469 were heated in an 80 ºC water bath for 1.5 hours, with 15 seconds of vortexing every 30 minutes.
470 Methanol concentration of each sample was diluted to 10% by adding 45 mL of water, and cell
471 debris was pelleted by centrifugation at 4,000 g for 10 mins. The supernatants were used for the
472 subsequent steps.

473 All of the following steps were carried out in darkened rooms illuminated with red light to preserve
474 light-sensitive adenosylated corrinoid samples. Solid-phase extraction of adenosylated corrinoids
475 with Sep-Pak C18 cartridges (Waters) was performed as previously described (Sokolovskaya et
476 al., 2019). Solvents were evaporated in a vacuum concentrator centrifuge (Savant SPD1010,
477 Thermo Scientific) at 45 ºC and the samples were resuspended in 500 µL deionized water and
478 passed through 0.45 µm pore-size filters (Millex-HV, MilliporeSigma).

479 Corrinoids were analyzed on an Agilent 1200 series (high-performance liquid chromatography
480 system equipped with a diode array detector (Agilent Technologies). Samples were injected into
481 an Agilent Zorbax SB-Aq column (5-µm pore size, 4.6 by 150 mm). The following HPLC method
482 was used: solvent A, 0.1% formic acid–deionized water; solvent B, 0.1% formic acid–methanol;
483 flow rate of 1 mL/minute at 30°C; 25% to 34% solvent B for 11 minutes, followed by a linear
484 gradient of 34% to 50% solvent B over 2 minutes, followed by a linear gradient of 50% to 75%
485 solvent B over 8 minutes.

486 *Riboswitch fluorescent reporter assays*

487 Corrinoid dose-response assays of riboswitch reporter strains were set up as follows. Saturated
488 cultures of the riboswitch reporter strain in LB were diluted 200-fold in LB and dispensed into 96-
489 well microtiter plates (Corning Costar Assay Plate 3904) containing a range of concentrations of
490 various corrinoids. The plates were sealed with gas diffusible membranes (Breathe-Easy) and
491 incubated at 37 ºC for 4 to 5 hours in a benchtop heated plate shaker (Southwest Science) at 1,200
492 revolution per minute (rpm). GFP fluorescence (excitation/emission/bandwidth = 485 / 525 / 10
493 nm) and absorbance at 600 nm (A_{600}) were measured on a Tecan Infinite M1000 Pro plate reader.

494 The A_{600} measurements of uninoculated medium and fluorescence measurements of the parental
495 control strains lacking *gfp* were subtracted from all readings. Data were plotted and analyzed in
496 GraphPad Prism 9.

497 *3D structural analysis of corrinoids and macromolecular models*

498 Molecular models of base-on and base-off/His-on forms of cobalamin in complex with various
499 proteins and RNAs were downloaded from the Protein DataBank (PDB) (Table S1) (Berman et
500 al., 2000). PDB files were analyzed in UCSF Chimera 1.14 (Pettersen et al., 2004). Corrinoid
501 molecular models were aligned with each other by the central cobalt atom and coordinating
502 nitrogen atoms of the corrin ring, using the PDB ID 4GMA Cbl model as a reference. Corrinoid
503 models were aligned and within the binding sites of riboswitch structures PDB IDs 4GMA, 4FRN,
504 4GXY, and 6VMY (Chan and Mondragón, 2020; Johnson et al., 2012; Peselis and Serganov,
505 2013).

506 *Methionine-dependent growth of* B. subtilis *strains*

507 *B. subtilis* strains were streaked from frozen stocks onto LB agar plates and incubated overnight
508 at 37 ºC for 14-18 hrs. Single colonies were used to inoculate 3 mL liquid starter cultures
509 containing Spizizen minimal medium supplemented with 0.02% D-glucose and 0.2% L-Histidine
510 (SMM) (Anagnostopoulos and Spizizen, 1961). Starter cultures of the *metH*-expressing strains
511 were supplemented with 1 nM CNCbl to support growth. Starter cultures were incubated overnight
512 shaking (250 rpm, 37 ºC) for 20 hours, reaching cell density of about OD_{600} = 1.0. Starter cultures
513 were diluted 500-fold by transferring 50 µL of starter culture to 25 mL of SMM. Then 75 µL of
514 the diluted culture were dispensed into wells of a 96 well microtiter plate supplemented with 20
515 nM of various corrinoids. Plates were sealed with gas diffusible membranes (Breathe-Easy,
516 MilliporeSigma) and incubated at 37 ºC on the 'high shaking' setting of a BioTek Synergy2 plate
517 reader. Growth kinetics and *metE* and *metH* expression were measured by A_{600} and GFP
518 fluorescence every 15 minutes for 72 hours. Data were plotted and analyzed in GraphPad Prism 9.

519

520 **Acknowledgments**

521 We thank past and present members of the Taga lab for support. In particular, we thank Sebastian
522 Gude, Zachary Hallberg, and Gordon Pherribo for critical reading of the manuscript; Alexa Nicolas
523 and Amanda Shelton for helpful discussions; Anna Grimaldo and Jong-Duk Park for reagents. We
524 thank Amrita Hazra, Arash Komeili, Michael Marletta, Kathleen Ryan, and Matthew Traxler for
525 helpful discussions. We especially thank Ming Hammond for critical reading of the manuscript
526 and helpful advice. We are grateful to the labs of Benjamin Blackman, John Deuber, Krishna
527 Niyogi, and Matthew Traxler for use of their equipment. This work was supported by NIH grants
528 R01GM114535 and R35GM139633 to M.E.T. We acknowledge that this work was conducted on
529 the ancestral and unceded land of the Ohlone people.

530

531 **Author contributions**

Conceptualization, K.J.K., F.J.W., K.C.M., and M.E.T.; Methodology, K.J.K., O.M.S., K.C.M., and M.E.T.; Validation: R.R.P.; Investigation, K.J.K. and V.L.I.; Writing – Original Draft, K.J.K. and M.E.T.; Writing – Review & Editing, K.J.K., O.M.S., K.C.M., and M.E.T.; Funding Acquisition, M.E.T.; Resources, O.M.S. and K.C.M.; Supervision, M.E.T.

Declaration of interests

The authors declare no competing interests.

539 **References**

540 Allen, K.D., and Wang, S.C. (2014). Initial characterization of Fom3 from Streptomyces
541 wedmorensis: The methyltransferase in fosfomycin biosynthesis. Arch Biochem Biophys *543*, 67-
542 73.
543 Anagnostopoulos, C., and Spizizen, J. (1961). Requirements for transformation in Bacillus subtilis.
544 J Bacteriol *81*, 741-746.
545 Barker, H.A. (1985). beta-Methylaspartate-glutamate mutase from Clostridium tetanomorphum.
546 Methods Enzymol *113*, 121-133.
547 Barker, H.A., Smyth, R.D., Weissbach, H., Toohey, J.I., Ladd, J.N., and Volcani, B.E. (1960).
548 Isolation and properties of crystalline cobamide coenzymes containing benzimidazole or 5,6-
549 dimethylbenzimidazole. J Biol Chem *235*, 480-488.
550 Battersby, A.R. (2000). Tetrapyrroles: the pigments of life. Nat Prod Rep *17*, 507-526.
551 Berg, I.A., Kockelkorn, D., Buckel, W., and Fuchs, G. (2007). A 3-hydroxypropionate/4-
552 hydroxybutyrate autotrophic carbon dioxide assimilation pathway in Archaea. Science *318*, 1782-
553 1786.
554 Berkovitch, F., Behshad, E., Tang, K.H., Enns, E.A., Frey, P.A., and Drennan, C.L. (2004). A
555 locking mechanism preventing radical damage in the absence of substrate, as revealed by the x-
556 ray structure of lysine 5,6-aminomutase. Proc Natl Acad Sci U S A *101*, 15870-15875.
557 Berman, H.M., Westbrook, J., Feng, Z., Gilliland, G., Bhat, T.N., Weissig, H., Shindyalov, I.N.,
558 and Bourne, P.E. (2000). The Protein Data Bank. Nucleic Acids Research *28*, 235-242.
559 Bridwell-Rabb, J., Zhong, A., Sun, H.G., Drennan, C.L., and Liu, H.W. (2017). A B12-dependent
560 radical SAM enzyme involved in oxetanocin A biosynthesis. Nature *544*, 322-326.
561 Cech, Thomas R., and Steitz, Joan A. (2014). The Noncoding RNA Revolution - Trashing Old
562 Rules to Forge New Ones. Cell *157*, 77-94.
563 Chan, C.H., and Escalante-Semerena, J.C. (2012). ArsAB, a novel enzyme from *Sporomusa ovata*
564 activates phenolic bases for adenosylcobamide biosynthesis. Mol Microbiol *81*, 952-967.
565 Chan, C.H., Newmister, S.A., Talyor, K., Claas, K.R., Rayment, I., and Escalante-Semerena, J.C.
566 (2014). Dissecting cobamide diversity through structural and functional analyses of the base-
567 activating CobT enzyme of *Salmonella enterica*. Biochim Biophys Acta *1840*, 464-475.
568 Chan, C.W., and Mondragón, A. (2020). Crystal structure of an atypical cobalamin riboswitch
569 reveals RNA structural adaptability as basis for promiscuous ligand binding. Nucleic Acids Res
570 *48*, 7569-7583.
571 Chang, C.H., and Frey, P.A. (2000). Cloning, sequencing, heterologous expression, purification,
572 and characterization of adenosylcobalamin-dependent D-lysine 5, 6-aminomutase from
573 Clostridium sticklandii. J Biol Chem *275*, 106-114.
574 Chen, H.P., Wu, S.H., Lin, Y.L., Chen, C.M., and Tsay, S.S. (2001). Cloning, sequencing,
575 heterologous expression, purification, and characterization of adenosylcobalamin-dependent D-
576 ornithine aminomutase from Clostridium sticklandii. J Biol Chem *276*, 44744-44750.
577 Cheong, C.G., Escalante-Semerena, J.C., and Rayment, I. (1999). The three-dimensional
578 structures of nicotinate mononucleotide:5,6-dimethylbenzimidazole phosphoribosyltransferase
579 (CobT) from *Salmonella typhimurium* complexed with 5,6-dimethybenzimidazole and its reaction
580 products determined to 1.9 A resolution. Biochemistry *38*, 16125-16135.
581 Cheong, C.G., Escalante-Semerena, J.C., and Rayment, I. (2001). Structural investigation of the
582 biosynthesis of alternative lower ligands for cobamides by nicotinate mononucleotide:5,6-
583 dimethylbenzimidazole phosphoribosyltransferase from *Salmonella enterica*. J Biol Chem *276*,
584 37612-37620.

585 Choi, S.C., and Bartha, R. (1993). Cobalamin-mediated mercury methylation by *Desulfovibrio*
586 *desulfuricans* LS. Appl Environ Microbiol *59*, 290-295.
587 Choi, S.C., Chase, T., Jr., and Bartha, R. (1994). Enzymatic catalysis of mercury methylation by
588 Desulfovibrio desulfuricans LS. Appl Environ Microbiol *60*, 1342-1346.
589 Choudhary, P.K., Duret, A., Rohrbach-Brandt, E., Holliger, C., Sigel, R.K., and Maillard, J.
590 (2013). Diversity of cobalamin riboswitches in the corrinoid-producing organohalide respirer
591 *Desulfitobacterium hafniense*. J Bacteriol *195*, 5186-5195.
592 Crofts, T.S., Seth, E.C., Hazra, A.B., and Taga, M.E. (2013). Cobamide structure depends on both
593 lower ligand availability and CobT substrate specificity. Chem Biol *20*, 1265-1274.
594 Degnan, P.H., Barry, N.A., Mok, K.C., Taga, M.E., and Goodman, A.L. (2014). Human gut
595 microbes use multiple transporters to distinguish vitamin B12 analogs and compete in the gut. Cell
596 Host Microbe *15*, 47-57.
597 Dowling, D.P., Miles, Z.D., Köhrer, C., Maiocco, S.J., Elliott, S.J., Bandarian, V., and Drennan,
598 C.L. (2016). Molecular basis of cobalamin-dependent RNA modification. Nucleic Acids Res *44*,
599 9965-9976.
600 Drennan, C.L., Huang, S., Drummond, J.T., Matthews, R.G., and Ludwig, M.L. (1994). How a
601 protein binds B12: A 3.0 A X-ray structure of B12-binding domains of methionine synthase.
602 Science *266*, 1669-1674.
603 Erb, T.J., Rétey, J., Fuchs, G., and Alber, B.E. (2008). Ethylmalonyl-CoA mutase from
604 Rhodobacter sphaeroides defines a new subclade of coenzyme B12-dependent acyl-CoA mutases.
605 J Biol Chem *283*, 32283-32293.
606 Fedosov, S.N., Fedosova, N.U., Kräutler, B., Nexo, E., and Petersen, T.E. (2007). Mechanisms of
607 discrimination between cobalamins and their natural analogues during their binding to the specific
608 B12-transporting proteins. Biochemistry *46*, 6446-6458.
609 Ferguson, D.J., Jr., and Krzycki, J.A. (1997). Reconstitution of trimethylamine-dependent
610 coenzyme M methylation with the trimethylamine corrinoid protein and the isozymes of
611 methyltransferase II from Methanosarcina barkeri. J Bacteriol *179*, 846-852.
612 Fieber, W., Hoffmann, B., Schmidt, W., Stupperich, E., Konrat, R., and Kräutler, B. (2002).
613 Pseudocoenzyme B12 and adenosyl-Factor A: Electrochemical synthesis and spectroscopic
614 analysis of two natural B12 coenzymes with predominantly 'base-off' constitution. Helvetica
615 Chimica Acta *85*, 927-944.
616 Forage, R.G., and Foster, M.A. (1982). Glycerol fermentation in Klebsiella pneumoniae: functions
617 of the coenzyme B12-dependent glycerol and diol dehydratases. J Bacteriol *149*, 413-419.
618 Froese, D.S., Kochan, G., Muniz, J.R., Wu, X., Gileadi, C., Ugochukwu, E., Krysztofinska, E.,
619 Gravel, R.A., Oppermann, U., and Yue, W.W. (2010). Structures of the human GTPase MMAA
620 and vitamin B12-dependent methylmalonyl-CoA mutase and insight into their complex formation.
621 J Biol Chem *285*, 38204-38213.
622 Galizi, R., and Jaramillo, A. (2019). Engineering CRISPR guide RNA riboswitches for in vivo
623 applications. Curr Opin Biotechnol *55*, 103-113.
624 Gallo, S., Mundwiler, S., Alberto, R., and Sigel, R.K. (2011). The change of corrin-amides to
625 carboxylates leads to altered structures of the B12-responding *btuB* riboswitch. Chem Commun
626 (Camb) *47*, 403-405.
627 Gallo, S., Oberhuber, M., Sigel, R.K., and Kräutler, B. (2008). The corrin moiety of coenzyme
628 B12 is the determinant for switching the *btuB* riboswitch of *E. coli*. Chembiochem *9*, 1408-1414.

629 Gibson, D.G., Young, L., Chuang, R.-Y., Venter, J.C., Hutchison, C.A., and Smith, H.O. (2009).
630 Enzymatic assembly of DNA molecules up to several hundred kilobases. Nature methods *6*, 343-
631 345.
632 Gruber, K., Reitzer, R., and Kratky, C. (2001). Radical shuttling in a protein: Ribose
633 pseudorotation controls alkyl-radical transfer in the coenzyme B12-dependent enzyme glutamate
634 mutase. Angewandte Chemie International Edition *40*, 3377-3380.
635 Guiziou, S., Sauveplane, V., Chang, H.J., Clerté, C., Declerck, N., Jules, M., and Bonnet, J. (2016).
636 A part toolbox to tune genetic expression in Bacillus subtilis. Nucleic Acids Res *44*, 7495-7508.
637 Gusarov, I., and Nudler, E. (1999). The mechanism of intrinsic transcription termination. Mol Cell
638 *3*, 495-504.
639 Hallberg, Z.F., Su, Y., Kitto, R.Z., and Hammond, M.C. (2017). Engineering and In Vivo
640 Applications of Riboswitches. Annu Rev Biochem *86*, 515-539.
641 Hazra, A.B., Han, A.W., Mehta, A.P., Mok, K.C., Osadchiy, V., Begley, T.P., and Taga, M.E.
642 (2015). Anaerobic biosynthesis of the lower ligand of vitamin B12. Proc Natl Acad Sci U S A *112*,
643 10792-10797.
644 Hazra, A.B., Tran, J.L., Crofts, T.S., and Taga, M.E. (2013). Analysis of substrate specificity in
645 CobT homologs reveals widespread preference for DMB, the lower axial ligand of vitamin B12.
646 Chem Biol *20*, 1275-1285.
647 Helliwell, K.E., Lawrence, A.D., Holzer, A., Kudahl, U.J., Sasso, S., Kräutler, B., Scanlan, D.J.,
648 Warren, M.J., and Smith, A.G. (2016). Cyanobacteria and eukaryotic algae use different chemical
649 variants of vitamin B12. Curr Biol *26*, 999-1008.
650 Hoffmann, B., Oberhuber, M., Stupperich, E., Bothe, H., Buckel, W., Konrat, R., and Kräutler, B.
651 (2000). Native corrinoids from *Clostridium cochlearium* are adeninylcobamides: spectroscopic
652 analysis and identification of pseudovitamin B12 and factor A. J Bacteriol *182*, 4773-4782.
653 Huang, L., Liao, T.W., Wang, J., Ha, T., and Lilley, D.M.J. (2020). Crystal structure and ligand-
654 induced folding of the SAM/SAH riboswitch. Nucleic Acids Res *48*, 7545-7556.
655 Jeter, R.M. (1990). Cobalamin-dependent 1,2-propanediol utilization by Salmonella typhimurium.
656 J Gen Microbiol *136*, 887-896.
657 Johnson, J.E., Jr., Reyes, F.E., Polaski, J.T., and Batey, R.T. (2012). B12 cofactors directly
658 stabilize an mRNA regulatory switch. Nature *492*, 133-137.
659 Jost, M., Born, D.A., Cracan, V., Banerjee, R., and Drennan, C.L. (2015a). Structural Basis for
660 Substrate Specificity in Adenosylcobalamin-dependent Isobutyryl-CoA Mutase and Related Acyl-
661 CoA Mutases. J Biol Chem *290*, 26882-26898.
662 Jost, M., Fernández-Zapata, J., Polanco, M.C., Ortiz-Guerrero, J.M., Chen, P.Y., Kang, G.,
663 Padmanabhan, S., Elías-Arnanz, M., and Drennan, C.L. (2015b). Structural basis for gene
664 regulation by a B12-dependent photoreceptor. Nature *526*, 536-541.
665 Kennedy, K.J., and Taga, M.E. (2020). Cobamides. Curr Biol *30*, R55-r56.
666 Kim, H.J., McCarty, R.M., Ogasawara, Y., Liu, Y.N., Mansoorabadi, S.O., LeVieux, J., and Liu,
667 H.W. (2013). GenK-catalyzed C-6' methylation in the biosynthesis of gentamicin: isolation and
668 characterization of a cobalamin-dependent radical SAM enzyme. J Am Chem Soc *135*, 8093-8096.
669 Knox, H.L., Chen, P.Y., Blaszczyk, A.J., Mukherjee, A., Grove, T.L., Schwalm, E.L., Wang, B.,
670 Drennan, C.L., and Booker, S.J. (2021). Structural basis for non-radical catalysis by TsrM, a
671 radical SAM methylase. Nat Chem Biol *17*, 485-491.
672 Koo, B.M., Kritikos, G., Farelli, J.D., Todor, H., Tong, K., Kimsey, H., Wapinski, I., Galardini,
673 M., Cabal, A., Peters, J.M., *et al.* (2017). Construction and Analysis of Two Genome-Scale
674 Deletion Libraries for Bacillus subtilis. Cell Syst *4*, 291-305.e297.

675 Korotkova, N., Chistoserdova, L., Kuksa, V., and Lidstrom, M.E. (2002). Glyoxylate regeneration
676 pathway in the methylotroph Methylobacterium extorquens AM1. J Bacteriol *184*, 1750-1758.
677 Krasotkina, J., Walters, T., Maruya, K.A., and Ragsdale, S.W. (2001). Characterization of the B12-
678 and iron-sulfur-containing reductive dehalogenase from Desulfitobacterium chlororespirans. J
679 Biol Chem *276*, 40991-40997.
680 Kräutler, B. (2020). Antivitamins B12 - Some Inaugural Milestones. Chemistry *26*, 15438-15445.
681 Ladd, J.N., Hogenkamp, H.P., and Barker, H.A. (1961). Structure of cobamide coenzymes:
682 influence of pH on absorption spectra and ionophoretic mobilities. J Biol Chem *236*, 2114-2118.
683 Licht, S., Gerfen, G.J., and Stubbe, J. (1996). Thiyl radicals in ribonucleotide reductases. Science
684 *271*, 477-481.
685 Ljungdahl, L.G. (1986). The autotrophic pathway of acetate synthesis in acetogenic bacteria. Annu
686 Rev Microbiol *40*, 415-450.
687 Lussier, A., Bastet, L., Chauvier, A., and Lafontaine, D.A. (2015). A kissing loop is important for
688 btuB riboswitch ligand sensing and regulatory control. J Biol Chem *290*, 26739-26751.
689 Ma, A.T., Tyrell, B., and Beld, J. (2020). Specificity of cobamide remodeling, uptake and
690 utilization in Vibrio cholerae. Molecular Microbiology *113*, 89-102.
691 Ma, B., Bai, G., Nussinov, R., Ding, J., and Wang, Y.X. (2021). Conformational Ensemble of
692 TteAdoCbl Riboswitch Provides Stable Structural Elements for Conformation Selection and
693 Population Shift in Cobalamin Recognition. The journal of physical chemistry B *125*, 2589-2596.
694 Mancia, F., Keep, N.H., Nakagawa, A., Leadlay, P.F., McSweeney, S., Rasmussen, B., Bosecke,
695 P., Diat, O., and Evans, P.R. (1996). How coenzyme B12 radicals are generated: the crystal
696 structure of methylmalonyl-coenzyme A mutase at 2 A resolution. Structure *4*, 339-350.
697 Mansjö, M., and Johansson, J. (2011). The riboflavin analog roseoflavin targets an FMN-
698 riboswitch and blocks Listeria monocytogenes growth, but also stimulates virulence gene-
699 expression and infection. RNA Biol *8*, 674-680.
700 Marous, D.R., Lloyd, E.P., Buller, A.R., Moshos, K.A., Grove, T.L., Blaszczyk, A.J., Booker, S.J.,
701 and Townsend, C.A. (2015). Consecutive radical S-adenosylmethionine methylations form the
702 ethyl side chain in thienamycin biosynthesis. Proc Natl Acad Sci U S A *112*, 10354-10358.
703 Marques, H.M., Zou, X., and Brown, K.L. (2000). The solution structure of adenosylcobalamin
704 and adenosylcobinamide determined by nOe-restrained molecular dynamics simulations. Journal
705 of Molecular Structure *520*, 75-95.
706 Mathews, D.H., Disney, M.D., Childs, J.L., Schroeder, S.J., Zuker, M., and Turner, D.H. (2004).
707 Incorporating chemical modification constraints into a dynamic programming algorithm for
708 prediction of RNA secondary structure. Proc Natl Acad Sci U S A *101*, 7287-7292.
709 McCown, P.J., Corbino, K.A., Stav, S., Sherlock, M.E., and Breaker, R.R. (2017). Riboswitch
710 diversity and distribution. RNA *23*, 995-1011.
711 Mok, K.C., Sokolovskaya, O.M., Nicolas, A.M., Hallberg, Z.F., Deutschbauer, A., Carlson, H.K.,
712 and Taga, M.E. (2020). Identification of a novel cobamide remodeling enzyme in the beneficial
713 human gut bacterium *Akkermansia muciniphila*. mBio *11*, e02507-02520.
714 Mok, K.C., and Taga, M.E. (2013). Growth Inhibition of *Sporomusa ovata* by Incorporation of
715 Benzimidazole Bases into Cobamides. J Bacteriol *195*, 1902-1911.
716 Moore, S.J., Lawrence, A.D., Biedendieck, R., Deery, E., Frank, S., Howard, M.J., Rigby, S.E.,
717 and Warren, M.J. (2013). Elucidation of the anaerobic pathway for the corrin component of
718 cobalamin (vitamin B12). Proc Natl Acad Sci U S A *110*, 14906-14911.

Mukherjee, S., Das Mandal, S., Gupta, N., Drory-Retwitzer, M., Barash, D., and Sengupta, S. (2019). RiboD: a comprehensive database for prokaryotic riboswitches. Bioinformatics *35*, 3541-3543.

Mukherjee, S., and Sengupta, S. (2016). Riboswitch Scanner: an efficient pHMM-based web-server to detect riboswitches in genomic sequences. Bioinformatics *32*, 776-778.

Nahvi, A., Barrick, J.E., and Breaker, R.R. (2004). Coenzyme B12 riboswitches are widespread genetic control elements in prokaryotes. Nucleic Acids Res *32*, 143-150.

Nahvi, A., Sudarsan, N., Ebert, M.S., Zou, X., Brown, K.L., and Breaker, R.R. (2002). Genetic control by a metabolite binding mRNA. Chem Biol *9*, 1043.

Newmister, S.A., Chan, C.H., Escalante-Semerena, J.C., and Rayment, I. (2012). Structural insights into the function of the nicotinate mononucleotide:phenol/p-cresol phosphoribosyltransferase (ArsAB) enzyme from *Sporomusa ovata*. Biochemistry *51*, 8571-8582.

Panchal, V., and Brenk, R. (2021). Riboswitches as Drug Targets for Antibiotics. Antibiotics (Basel, Switzerland) *10*.

Parks, J.M., Johs, A., Podar, M., Bridou, R., Hurt, R.A., Jr., Smith, S.D., Tomanicek, S.J., Qian, Y., Brown, S.D., Brandt, C.C.*, et al.* (2013). The genetic basis for bacterial mercury methylation. Science *339*, 1332-1335.

Pavlova, N., Kaloudas, D., and Penchovsky, R. (2019). Riboswitch distribution, structure, and function in bacteria. Gene *708*, 38-48.

Payne, K.A., Fisher, K., Sjuts, H., Dunstan, M.S., Bellina, B., Johannissen, L., Barran, P., Hay, S., Rigby, S.E., and Leys, D. (2015a). Epoxyqueuosine Reductase Structure Suggests a Mechanism for Cobalamin-dependent tRNA Modification. J Biol Chem *290*, 27572-27581.

Payne, K.A., Quezada, C.P., Fisher, K., Dunstan, M.S., Collins, F.A., Sjuts, H., Levy, C., Hay, S., Rigby, S.E., and Leys, D. (2015b). Reductive dehalogenase structure suggests a mechanism for B12-dependent dehalogenation. Nature *517*, 513-516.

Peselis, A., and Serganov, A. (2013). Structural insights into ligand binding and gene expression control by an adenosylcobalamin riboswitch. Nat Struct Mol Biol *19*, 1182-1184.

Pettersen, E.F., Goddard, T.D., Huang, C.C., Couch, G.S., Greenblatt, D.M., Meng, E.C., and Ferrin, T.E. (2004). UCSF Chimera--a visualization system for exploratory research and analysis. Journal of computational chemistry *25*, 1605-1612.

Pierre, S., Guillot, A., Benjdia, A., Sandström, C., Langella, P., and Berteau, O. (2012). Thiostrepton tryptophan methyltransferase expands the chemistry of radical SAM enzymes. Nat Chem Biol *8*, 957-959.

Polaski, J.T., Holmstrom, E.D., Nesbitt, D.J., and Batey, R.T. (2016). Mechanistic Insights into Cofactor-Dependent Coupling of RNA Folding and mRNA Transcription/Translation by a Cobalamin Riboswitch. Cell Rep *15*, 1100-1110.

Polaski, J.T., Kletzien, O.A., Drogalis, L.K., and Batey, R.T. (2018). A functional genetic screen reveals sequence preferences within a key tertiary interaction in cobalamin riboswitches required for ligand selectivity. Nucleic Acids Res *46*, 9094-9105.

Polaski, J.T., Webster, S.M., Johnson, J.E., Jr., and Batey, R.T. (2017). Cobalamin riboswitches exhibit a broad range of ability to discriminate between methylcobalamin and adenosylcobalamin. J Biol Chem *292*, 11650-11658.

Price, I.R., Grigg, J.C., and Ke, A. (2014). Common themes and differences in SAM recognition among SAM riboswitches. Biochim Biophys Acta *1839*, 931-938.

Quereda, J.J., and Cossart, P. (2017). Regulating Bacterial Virulence with RNA. Annu Rev Microbiol *71*, 263-280.

765 Reuter, J.S., and Mathews, D.H. (2010). RNAstructure: software for RNA secondary structure
766 prediction and analysis. BMC Bioinformatics *11*, 129.
767 Rodionov, D.A., Vitreschak, A.G., Mironov, A.A., and Gelfand, M.S. (2003). Comparative
768 genomics of the vitamin B12 metabolism and regulation in prokaryotes. J Biol Chem *278*, 41148-
769 41159.
770 Romine, M.F., Rodionov, D.A., Maezato, Y., Anderson, L.N., Nandhikonda, P., Rodionova, I.A.,
771 Carre, A., Li, X., Xu, C., Clauss, T.R.*, et al.* (2017). Elucidation of roles for vitamin B12 in
772 regulation of folate, ubiquinone, and methionine metabolism. Proc Natl Acad Sci U S A *114*,
773 E1205-e1214.
774 Roth, A., and Breaker, R.R. (2009). The structural and functional diversity of metabolite-binding
775 riboswitches. Annu Rev Biochem *78*, 305-334.
776 Scarlett, F.A., and Turner, J.M. (1976). Microbial metabolism of amino alcohols. Ethanolamine
777 catabolism mediated by coenzyme B12-dependent ethanolamine ammonia-lyase in Escherichia
778 coli and Klebsiella aerogenes. J Gen Microbiol *95*, 173-176.
779 Shelton, A.N., Lyu, X., and Taga, M.E. (2020). Flexible cobamide metabolism in *Clostridioides*
780 (*Clostridium*) *difficile* 630 Δerm. J Bacteriol *202*.
781 Shelton, A.N., Seth, E.C., Mok, K.C., Han, A.W., Jackson, S.N., Haft, D.R., and Taga, M.E.
782 (2019). Uneven distribution of cobamide biosynthesis and dependence in bacteria predicted by
783 comparative genomics. ISME J *13*, 789-804.
784 Singh, P., Bandyopadhyay, P., Bhattacharya, S., Krishnamachari, A., and Sengupta, S. (2009).
785 Riboswitch detection using profile hidden Markov models. BMC Bioinformatics *10*, 325.
786 Sokolovskaya, O.M., Mok, K.C., Park, J.D., Tran, J.L.A., Quanstrom, K.A., and Taga, M.E.
787 (2019). Cofactor Selectivity in Methylmalonyl Coenzyme A Mutase, a Model Cobamide-
788 Dependent Enzyme. mBio *10*, e01303-01319.
789 Sokolovskaya, O.M., Plessl, T., Bailey, H., Mackinnon, S., Baumgartner, M.R., Yue, W.W.,
790 Froese, D.S., and Taga, M.E. (2020). Naturally occurring cobalamin (B12) analogs can function
791 as cofactors for human methylmalonyl-CoA mutase. Biochimie.
792 Stupperich, E., Eisinger, H.J., and Kräutler, B. (1988). Diversity of corrinoids in acetogenic
793 bacteria. P-cresolylcobamide from *Sporomusa ovata*, 5-methoxy-6-
794 methylbenzimidazolylcobamide from *Clostridium formicoaceticum* and vitamin B12 from
795 *Acetobacterium woodii*. Eur J Biochem *172*, 459-464.
796 Stupperich, E., and Konle, R. (1993). Corrinoid-Dependent Methyl Transfer Reactions Are
797 Involved in Methanol and 3,4-Dimethoxybenzoate Metabolism by Sporomusa ovata. Appl
798 Environ Microbiol *59*, 3110-3116.
799 Sudarsan, N., Hammond, M.C., Block, K.F., Welz, R., Barrick, J.E., Roth, A., and Breaker, R.R.
800 (2006). Tandem riboswitch architectures exhibit complex gene control functions. Science *314*,
801 300-304.
802 Sussman, D., and Wilson, C. (2000). A water channel in the core of the vitamin B12 RNA aptamer.
803 Structure *8*, 719-727.
804 Takano, H., Kondo, M., Usui, N., Usui, T., Ohzeki, H., Yamazaki, R., Washioka, M., Nakamura,
805 A., Hoshino, T., Hakamata, W.*, et al.* (2011). Involvement of CarA/LitR and CRP/FNR family
806 transcriptional regulators in light-induced carotenoid production in Thermus thermophilus. J
807 Bacteriol *193*, 2451-2459.
808 Takano, H., Mise, K., Hagiwara, K., Hirata, N., Watanabe, S., Toriyabe, M., Shiratori-Takano, H.,
809 and Ueda, K. (2015). Role and Function of LitR, an Adenosyl B12-Bound Light-Sensitive

Regulator of Bacillus megaterium QM B1551, in Regulation of Carotenoid Production. J Bacteriol *197*, 2301-2315.

Tanioka, Y., Miyamoto, E., Yabuta, Y., Ohnishi, K., Fujita, T., Yamaji, R., Misono, H., Shigeoka, S., Nakano, Y., Inui, H.*, et al.* (2010). Methyladeninylcobamide functions as the cofactor of methionine synthase in a Cyanobacterium, *Spirulina platensis* NIES-39. FEBS Lett *584*, 3223-3226.

Trausch, J.J., and Batey, R.T. (2014). A disconnect between high-affinity binding and efficient regulation by antifolates and purines in the tetrahydrofolate riboswitch. Chem Biol *21*, 205-216.

Trzebiatowski, J.R., and Escalante-Semerena, J.C. (1997). Purification and characterization of CobT, the nicotinate-mononucleotide:5,6-dimethylbenzimidazole phosphoribosyltransferase enzyme from *Salmonella typhimurium* LT2. J Biol Chem *272*, 17662-17667.

Trzebiatowski, J.R., O'Toole, G.A., and Escalante-Semerena, J.C. (1994). The *cobT* gene of *Salmonella typhimurium* encodes the NaMN: 5,6-dimethylbenzimidazole phosphoribosyltransferase responsible for the synthesis of N1-(5-phospho-alpha-D-ribosyl)-5,6-dimethylbenzimidazole, an intermediate in the synthesis of the nucleotide loop of cobalamin. J Bacteriol *176*, 3568-3575.

Villa, J.K., Su, Y., Contreras, L.M., and Hammond, M.C. (2018). Synthetic Biology of Small RNAs and Riboswitches. Microbiol Spectr *6*.

Wang, P.H., Chen, Y.L., Wei, S.T., Wu, K., Lee, T.H., Wu, T.Y., and Chiang, Y.R. (2020). Retroconversion of estrogens into androgens by bacteria via a cobalamin-mediated methylation. Proc Natl Acad Sci U S A *117*, 1395-1403.

Waterhouse, A.M., Procter, J.B., Martin, D.M., Clamp, M., and Barton, G.J. (2009). Jalview Version 2--a multiple sequence alignment editor and analysis workbench. Bioinformatics *25*, 1189-1191.

Weickhmann, A.K., Keller, H., Wurm, J.P., Strebitzer, E., Juen, M.A., Kremser, J., Weinberg, Z., Kreutz, C., Duchardt-Ferner, E., and Wöhnert, J. (2019). The structure of the SAM/SAH-binding riboswitch. Nucleic Acids Res *47*, 2654-2665.

Wilson, K.S., and von Hippel, P.H. (1995). Transcription termination at intrinsic terminators: the role of the RNA hairpin. Proc Natl Acad Sci U S A *92*, 8793-8797.

Winkler, W.C., and Breaker, R.R. (2005). Regulation of bacterial gene expression by riboswitches. Annu Rev Microbiol *59*, 487-517.

Wrist, A., Sun, W., and Summers, R.M. (2020). The theophylline aptamer: 25 years as an important tool in cellular engineering research. ACS Synth Biol *9*, 682-697.

Yan, J., Bi, M., Bourdon, A.K., Farmer, A.T., Wang, P.H., Molenda, O., Quaile, A.T., Jiang, N., Yang, Y., Yin, Y.*, et al.* (2018). Purinyl-cobamide is a native prosthetic group of reductive dehalogenases. Nat Chem Biol *14*, 8-14.

Yi, S., Seth, E.C., Men, Y.J., Stabler, S.P., Allen, R.H., Alvarez-Cohen, L., and Taga, M.E. (2012). Versatility in corrinoid salvaging and remodeling pathways supports corrinoid-dependent metabolism in *Dehalococcoides mccartyi*. Appl Environ Microbiol *78*, 7745-7752.

Zelder, F., Sonnay, M., and Prieto, L. (2015). Antivitamins for Medicinal Applications. Chembiochem *16*, 1264-1278.

Zhang, X.Z., and Zhang, Y. (2011). Simple, fast and high-efficiency transformation system for directed evolution of cellulase in Bacillus subtilis. Microb Biotechnol *4*, 98-105.